

Census of the Local Universe (CLU) I: Characterization of Galaxy Catalogs from Preliminary Fields

David O. Cook,¹ Mansi M. Kasliwal,¹ Angela Van Sistine,² David L. Kaplan,² Jessica S. Sutter,³ Thomas Kupfer,¹ David L. Shupe,⁴ Russ R. Laher,⁴ Frank J. Masci,⁴ Daniel A. Dale,³ Branimir Sesar⁵ Patrick R. Brady,² Lin Yan,⁴ Eran O. Ofek,⁶

¹ California Institute of Technology, 1200 East California Blvd, Pasadena, CA 91125, USA; dcook@astro.caltech.edu

² University of Wisconsin-Milwaukee, P.O. Box 413, Milwaukee, WI 53201, USA

³ University of Wyoming, 1000 University Ave, Laramie, WY 82071, USA

⁴ Infrared Processing and Analysis Center, California Institute of Technology, Pasadena, CA 91125, U.S.A.

⁵ Max Planck Institute for Astronomy, Knigstuhl 17, D-69117 Heidelberg, Germany

⁶ Weizmann Institute of Science, Rehovot, Israel

16 October 2017

ABSTRACT

We present a Census of the Local Universe (CLU) – a combination of the largest area H α imaging survey for nearby emission-line galaxies to date as well as a compilation of all publicly available galaxy catalogs out to a distance of 200 Mpc. With the Palomar 48-inch telescope, our H α survey images $\approx 3\pi$ of the sky (3626 pointings) in 4 narrowband filters to an H α flux limit of 10^{-14} erg/s/cm 2 at 90% completeness. To characterize the completeness and contamination of the H α survey, we undertook a study of 14 preliminary fields (0.3% of total pointings) where we have obtained spectroscopic follow-up of all galaxy candidates with no previous distance information and a narrow-band color excess greater than 2.5σ . Comparison of the resulting CLU-H α galaxy catalog to a statistically complete sample of star-forming galaxies in an 11 Mpc volume (the LVL sample), we find that the H α survey is complete to 85% in star-formation (using extinction corrected H α flux as a proxy) and 70% in stellar mass at 200 Mpc. The contamination from high-redshift galaxies is lower than 8% (40%) for a 5σ (2.5σ) color excess. Even with just 290 emission-line galaxies in the 14 preliminary fields, we find several interesting objects: 7 newly discovered blue compact dwarfs (aka, blueberries), 1 new green pea, 1 new QSO, and a known planetary nebula. The extreme galaxies (green pea and blueberries) have high star formation rates, low stellar masses, and low metallicities and could be local analogs to higher redshift primordial galaxies. The existence of these interesting candidates in our preliminary H α sample exemplifies that the full CLU-H α survey can be used as a discovery machine for a wide variety of objects in our own Galaxy and extreme galaxies out to intermediate redshifts.

Key words: galaxies: dwarf – galaxies: irregular – Local Group – galaxies: spiral – galaxies: star formation

1 INTRODUCTION

We are undertaking the Census of the Local Universe (CLU) project to build a complete catalog of galaxies out to 200 Mpc. As a first step, we compiled all known galaxies with secure redshifts within 200 Mpc, hereafter the CLU-compiled catalog (see Section 4.7). As the next step, we un-

dertook an emission-line survey to identify missing galaxies in this same volume, hereafter CLU-H α . The CLU-H α survey deploys four contiguous narrow-band filters to search for emission-line galaxies across $\approx 3\pi$ of the sky, as part of the Palomar Transient Factory (PTF; Law et al. 2009). Using the H α emission line, the CLU-H α survey is designed to find galaxies from redshift 0 to 0.048 (≈ 200 Mpc). The galaxies

found in CLU-H α will impact several areas of astrophysical research (e.g., galaxy evolution, star formation, and distributions of Milky Way emission-line sources). The combined CLU catalog will help focus the search for electromagnetic (EM) counterparts to gravitational wave (GW) events.

1.1 Galaxy Evolution and Star Formation

Large area surveys have led to important discoveries in star formation and galaxy evolution. The Sloan Digital Sky Survey (SDSS; York et al. 2000) directly led to the discovery of the “Main Sequence” of star-forming galaxies, where the current star-formation rate (SFR) forms a tight relationship with the total stellar mass (Brinchmann et al. 2004; Daddi et al. 2007; Salim et al. 2007; Peng et al. 2010). This discovery led to further studies which found that the “Main Sequence” shows an increased normalization at higher redshifts (Elbaz et al. 2007; Noeske et al. 2007; Heinis et al. 2014) providing a means to quantify the evolution of galaxy properties over time.

The SDSS survey also gave rise to the discovery of extreme emission-line galaxies at intermediate redshifts ($0.11 \leq z \leq 0.36$) dubbed “green peas.” These objects were identified based on their point source-like appearance where the strong [OIII] $\lambda 4959, \lambda 5007$ doublet ($\text{EW} \geq 100 \text{ \AA}$) is located in the green-coded SDSS r-band filter giving them their green colors (Lintott et al. 2008). In depth studies of green peas have shown that these objects have compact morphologies, large SFRs, low stellar masses, and low metallicities (Cardamone et al. 2009; Amorín, Pérez-Montero & Vilchez 2010; Izotov, Guseva & Thuan 2011). Thus, these galaxies bear a striking resemblance to high-redshift galaxies (Lyman-break galaxies and Ly α emitters) that are thought to contribute a significant fraction of ionizing photons during the epoch of reionization (Finkelstein et al. 2012).

Later studies of extreme galaxies found in SDSS (Izotov, Guseva & Thuan 2011) characterized local Universe analogs of green peas with blue colors (i.e., blue compact dwarfs or “blueberries”) at $z < 0.07$, where the strong [OIII] $\lambda 4959, \lambda 5007$ lines are located in the blue-coded g-band SDSS filter. Izotov, Guseva & Thuan (2011) found that the physical properties of both green peas and blueberries are similar suggesting that both are rare and interesting analogs to higher-redshift galaxies with extreme star-formation properties. Green peas and blueberries are likely to be found in the CLU-H α survey, and will provide an opportunity to study in greater detail modes of star formation thought to be common only in the early Universe.

The SDSS spectroscopic galaxy survey obtained spectra of half a million extragalactic sources in $\sim 9400 \text{ deg}^2$ using fiber-fed plates (Alam et al. 2015). However, the incompleteness function of the SDSS spectroscopic catalog is hard to quantify and consequently has missed galaxies due to fiber collisions, classification errors, etc. (Fukugita et al. 2007). An ideal galaxy survey would provide both imaging as well as spectroscopic information for all objects (down to a given depth) over large areas of the sky. This can be accomplished via narrowband filters which probe strong emission lines. A survey of this magnitude and wealth of information could provide the data for future discoveries and scientific advancements in many area of astrophysical research.

A narrowband survey that covers tens of thousands

of square degrees could discover tens of thousands of new galaxies providing a better census of the local Universe. Furthermore, a large area, narrowband survey would discover new extreme objects that have only been found in relatively low numbers providing insights into star formation and galaxy evolution. In addition, a survey of this nature could also provide a better census of emission-lines sources in our own galaxy (planetary nebulae, nova shells, supernova remnants, etc.) if one narrowband filter coincided with the rest-frame H α wavelength.

Given these motivations, we undertook the CLU-H α narrowband survey with filters that cover the rest-frame H α emission line and extends out to a distance of 200 Mpc covering $\approx 3\pi$ of the sky. In this paper, we introduce the CLU-H α survey, provide the survey parameters (e.g., sky coverage, narrow-band filter properties, detection limits, and estimated completeness), detail the galaxy candidate selection criteria, show examples of extreme objects found in preliminary fields, and discuss science applications in these preliminary pointings. Future papers will provide science analyses for successively larger numbers of pointings (i.e., larger sky coverages), and finally for the full $\approx 3\pi$ survey with 3 stacked images on every point in the coverage map.

1.2 Gravitational Waves

The detection of gravitational waves via the Laser Interferometer Gravitational Wave Observatory (LIGO; Abbott et al. 2016) allows for a new way of observing the Universe and thus provides new tools with which to understand fundamental physics. Associating gravitational waves and electromagnetic counterparts will have dramatic impacts on our understanding of the Universe. However, the sky localization of LIGO GW events can range from 30-1000 square degrees on the sky making the search for EM counterparts a challenge.

Significant efforts of large area surveys (e.g., Kasliwal et al. 2016) have scanned the most probable sections of gravitational wave localizations in search of an electromagnetic counterpart. However, the efficiency of this effort can be greatly enhanced by utilizing the locations of known galaxies in the LIGO sensitivity volume ($D \leq 200 \text{ Mpc}$; Aasi et al. 2015). The total area of all known galaxies in this volume occupy $\sim 1\%$ of the sky (see § 4.7). Thus, targeted follow-up observations of likely host galaxies can narrow down the search area (or false positives) by a factor of 100.

Previous efforts have been made to provide lists of galaxies specifically designed for EMGW follow-up (Kopparapu et al. 2008; White et al. 2011), where the latest catalog from White et al. (2011) shows a B-band luminosity completeness of 65% at 100 Mpc. However, the galaxies in both previous catalogs were limited to 100 Mpc which is an eighth of the LIGO sensitivity volume out to 200 Mpc. In addition, several new or updated spectroscopic galaxy surveys have published secure distances via redshifts for new galaxies in the local Universe (e.g., SDSS, ALFALFA, 6dFRGS; Alam et al. 2015; Haynes et al. 2011; Jones et al. 2009); thus, leaving previous EMGW galaxy catalogs less complete than previously estimated. There are efforts which utilize increased numbers of galaxies with photometric redshifts (e.g.,

GLADE¹); however, we focus on galaxy catalogs with secure distance measurements. The lack of an EMGW catalog that extends to the full LIGO sensitivity volume and the existence of new galaxies found in the local Universe motivate the construction of a new compiled galaxy catalog to be used in the search for EM counterparts to GW events.

In an effort to provide the most complete list of galaxies with measured distances in the LIGO sensitivity volume, our team has compiled a catalog of all known galaxies (CLU-compiled). The compiled portion of the CLU galaxy catalog was taken from existing galaxy databases: NASA/IPAC Extragalactic Database (NED)², Hyperleda³ (Makarov et al. 2014), Extragalactic Distance Database⁴ (EDD; Tully et al. 2009), the Sloan digital sky survey DR12 (SDSS; Alam et al. 2015), The 2dF Galaxy Redshift Survey (6dFRGS; Jones et al. 2009), and The Arecibo Legacy Fast ALFA (ALFALFA Haynes et al. 2011). The catalog contains $\sim 234,500$ galaxies with existing distances less than 200 Mpc.

The combination of CLU-compiled with new CLU-H α galaxies will serve as the full CLU galaxy catalog. CLU aims to facilitate rapid associations between GW events and EM detections by providing a catalog of local Universe galaxies that is as complete as possible. In this paper, we provide the basic properties of our CLU-compiled catalog and investigate how the new galaxies from the CLU-H α survey will contribute to the full CLU catalog.

2 CLU-H α SURVEY DESCRIPTION

The CLU-H α survey endeavors to discover as many H α -emitting galaxies as possible out to 200 Mpc ($z=0.048$) and provide a relatively well constrained redshift range for each emission-line galaxy. In addition, the H α fluxes measured for all galaxies (both previously known and newly discovered in the local Universe) will provide a recent SFR for each galaxy (i.e., the integrated SFR over the past ~ 10 Myr; e.g., Kennicutt 1998; Murphy et al. 2011; Kennicutt & Evans 2012). Thus CLU-H α will not only yield the positions and well constrained distances for new galaxies in the local Universe, but will also provide nearly uniform H α fluxes and SFRs for both new and known galaxies.

2.1 Narrowband Filters

CLU-H α searches for emission-line galaxies using 4 wavelength-adjacent, narrowband filters with a combined wavelength range of 6525–6878 Å. Each emission-line galaxy can be identified via a flux excess in one filter (the “On” filter) signifying the presence of an emission line compared to a filter that covers only the adjacent continuum (the “Off” filter). Thus, CLU-H α provides a distance constrained by the width of our narrowband filters.

The transmission curves for our narrowband filters are shown in Figure 1, where the solid lines represent the transmission from the manufacturer, the dotted line represents

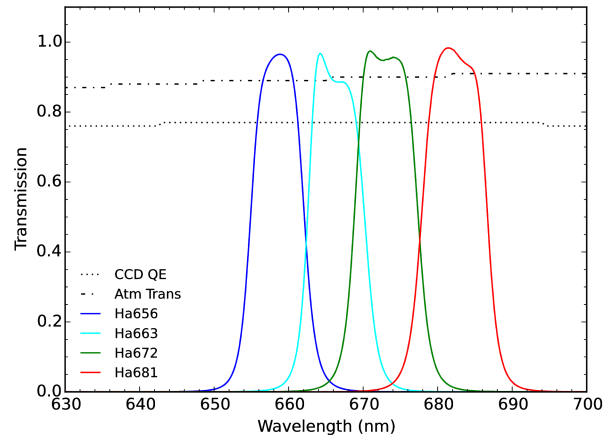


Figure 1. The measured filter transmission profiles of the 4 CLU-H α narrowband filters where the blue, cyan, green, and red curves represent H α 1, H α 2, H α 3, and H α 4 filters, respectively. The horizontal dotted and dashed lines represent the CCD quantum efficiency and the atmospheric transmission at Palomar Observatory, respectively.

the CCD quantum efficiency of the camera and the dash-dotted line represent the atmospheric transmission at Palomar (Ofek et al. 2012).

The filter widths and central wavelengths are calculated via:

$$\Delta\lambda \equiv \int T(\lambda)d\lambda, \quad (1)$$

$$\bar{\lambda} \equiv \frac{\int \lambda T(\lambda)d\lambda}{\int T(\lambda)d\lambda}, \quad (2)$$

where T is final transmittance of the filter curves with the peak normalized to unity. Table 1 presents the properties of our 4 narrowband filters.

The first filter is centered at the $z=0$ H α emission line ($\lambda = 6563$ Å) and the wavelength range of the last filter extends to $z \sim 0.048$ (i.e., ~ 200 Mpc) H α emission line. The first two filters (H α 1 and H α 2) make up the first filter pair and the 3rd and 4th filters (H α 3 and H α 4) make up the second filter pair. Each filter pair is observed per night to facilitate more stable H α “On-Off” colors used for emission-line selection (see §3).

2.2 Observational Strategy

Observations were taken on the Oschin 48 inch telescope at the Palomar Observatory with a 7.26 deg^2 mosaic imager composed of 11 CCD detectors (or chips) and a 1'' per pixel resolution (for details see, Law et al. 2009; Rau et al. 2009). The survey uses an observational strategy of 3 spatially-staggered, overlapping grids that are limited to a declination of greater than -20° , where each grid contains $N = 3626$ PTF fields ($26,470 \text{ deg}^2$ of the sky). Observations using the H α 1 and H α 2 filters cover the entire sky above -20° declination. Observations using the H α 3 and H α 4 filters also cover the sky above -20° declination, but avoid

¹ <http://aquarius.elte.hu/glade/>

² <https://ned.ipac.caltech.edu>

³ <http://leda.univ-lyon1.fr>

⁴ <http://edd.ifa.hawaii.edu>

Narrowband H α Filter Properties				
Filter Name	Filter $\bar{\lambda}$ (Å)	Filter $\Delta\lambda$ (Å)	Redshift range (#)	
H α 1	6562.4	76.2	-0.0059 < z < 0.0057	
H α 2	6642.4	78.5	0.0061 < z < 0.0181	
H α 3	6741.5	91.7	0.0202 < z < 0.0342	
H α 4	6832.3	92.0	0.0341 < z < 0.0480	

Table 1. The properties of the CLU narrowband filters, where the columns present the filter names, central wavelength, FWHM, and redshift range, from left-to-right. The first filter (H α 1) is centered on rest-frame H α while the last filter’s FWHM extends to 200 Mpc.

the Galactic plane ($|b| \gtrsim 3^\circ$). A single 60 second exposure is taken for each field in each grid resulting in a total of three images for each position on the sky. The multiple images facilitate cosmic ray rejection, filling in chip gaps, and deeper final images with 3 coadded images.

Data acquisition ended in March 2017 (due to decommissioning of the PTF camera) with 98.3% of fields observed in H α 1 and H α 2 and 91.3% observed in H α 3 and H α 4. However, the second filter pair is 95% completed at a Galactic latitude limit of three degrees (95% at $|b| \gtrsim 3^\circ$) and 99% completed at latitudes above 11° (99% at $|b| \gtrsim 11^\circ$). Figures 2 and 3 present the sky coverage maps in equatorial coordinates (where 0° Right Ascension is represented as the center, vertical red line) of the CLU-H α survey for the first filter pair (H α 1 and H α 2) and the second filter pair (H α 3 and H α 4), respectively. The colors for each PTF pointing box in these figures represent the number of observations, where lighter/brighter colors indicate more observations. The Galactic plane is easily identified in Figure 3 as a dark strip of fields with little to no observations in the second filter pair. The majority of the fields within our targeted sky coverage have 3 observations. In addition to our survey, there were multiple PTF projects that observed specific regions of the sky using the CLU narrowband filters and can provide even deeper H α imaging for these fields. The locations that these programs targeted are apparent in Figures 2 and 3 as the brightest regions with \sim 100-200 observations.

Although the ultimate goal of the CLU-H α survey is to coadd the images from the 3 staggered, overlapping grid patterns, the preliminary analysis here uses the single exposures from only one of these grids in 14 fields (see §3.1). Future investigations will provide analysis of additional, single-exposure images followed by analysis of the coadded images.

2.3 Data Reduction and Source Catalogs

Data reduction and source extraction are carried out in an automated pipeline built by the Infrared Processing and Analysis Center (IPAC)⁵ specifically for the PTF survey. The full description of this pipeline can be found in Laher et al. (2014), but we provide a brief overview here.

The IPAC reduction pipeline consists of both “off-the-shelf” and custom software which have been extensively

tested on millions of images from PTF broadband images. After each night of data is acquired, the IPAC pipeline performs a bias subtraction and applies a flat-field correction. The astrometric solution for each processed image is computed via **SCAMP** (Bertin 2006) on one of three stellar catalogs: SDSS-DR7 (Abazajian et al. 2009), UCAC3 (Zacharias et al. 2010), or USNO-B1 (Monet et al. 2003).

After data reduction is completed, the IPAC pipeline then uses **Source Extractor** (Bertin & Arnouts 1996) to generate a source catalog for every chip/filter image in each field. The fluxes are reported using many aperture definitions; however, we utilize the fluxes from aperture photometry at 5 pixels ($\sim 5''$) in diameter for galaxy candidate selection (see §3) and the point spread function (PSF) fitted fluxes of stars for calibration purposes (see below). The 5 pixel aperture used to select narrowband excess sources is ~ 2.5 times the FWHM of typical seeing ($2''$) at Palomar and will encompass $> 99\%$ of the light from a point source. The median and standard deviation 5σ detection limits of a point source with a $5''$ diameter aperture for each chip image in all 14 preliminary fields is 18.6 ± 0.30 , 18.7 ± 0.28 , 18.8 ± 0.28 , 18.8 ± 0.25 AB mag for filters H α 1, H α 2, H α 3, and H α 4, respectively.

2.4 Calibration

Calibration is carried out for each chip and filter image, where Pan-STARRS DR1 (PS1; Chambers et al. 2016) stars ($N > 100$) are matched with CLU-H α sources. We match all CLU-H α sources that are relatively isolated (i.e., no source within $10''$), have a photometric error less than 0.1 mag, and have no **Source Extractor** photometry flags to all PS1 stars with the following criteria: 1) a g-i color between 0 and 1.5 mag; 2) a photometric error less than 0.1 mag; 3) a PSF minus Kron i-band magnitude less than 0.05 mag to select stars⁶. The photometric zeropoints and color correction terms are determined by fitting a linear relationship between H α -r (CLU-PS1) and g-i (PS1-PS1) colors, where both CLU-H α and PS1 magnitudes are PSF fitted magnitudes.

Figure 4 graphically presents our calibration method, where the grey dots represent all CLU-H α sources matched to PS1 sources, the blue dots represent matched “good” stars that meet our criteria, the dashed line represents the zeropoint, and the solid-cyan line represents the fit to “good” stars. The scatter around the fit is used as the error in the zeropoint and is added in quadrature to each sources photometric error. Typical errors in the zeropoints are ~ 0.05 mag. In addition, the fitted line in Figure 4 is used to perform a color correction to the zeropoint.

There is also an effect of sensitivity across each of the chips due to the large field of view resulting in a variation in the zeropoint. The zeropoint variation across a single chip has a range of 0.001–0.004 mag (Van Sistine et al. in prep). The zeropoint variation maps are fully described and will be released in Van Sistine et al. (in prep).

⁵ <http://www.ipac.caltech.edu/>

⁶ <https://confluence.stsci.edu/display/PANSTARRS/How+to+separate+stars+and+galaxies>

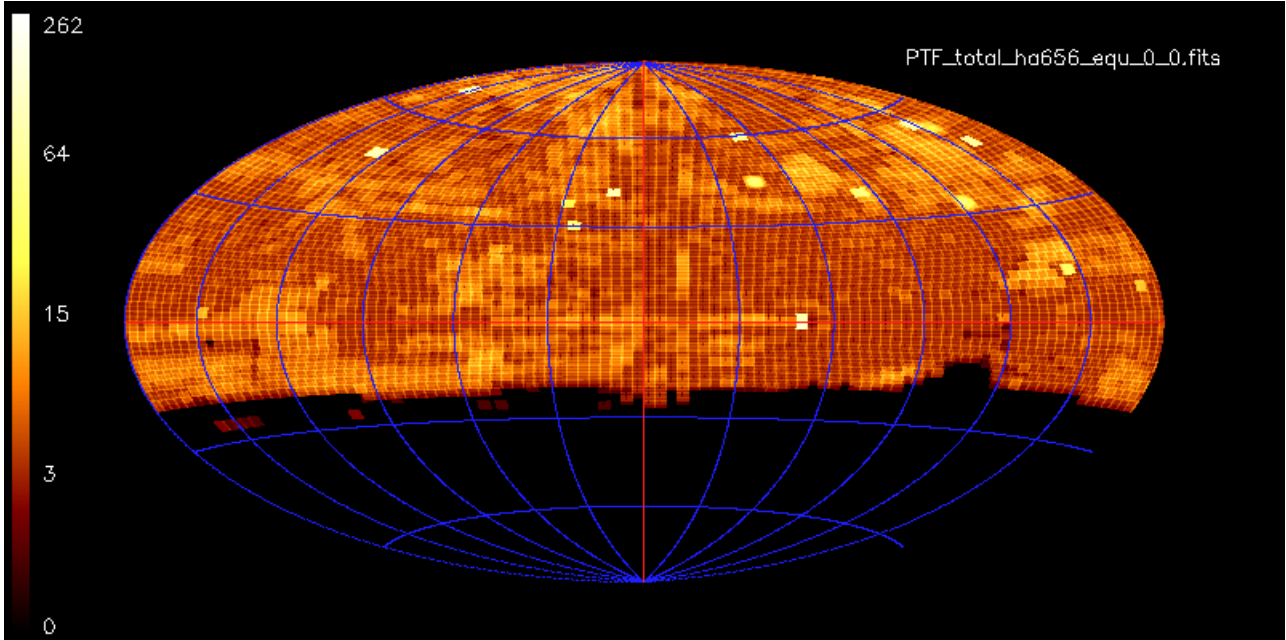


Figure 2. The sky coverage map in equatorial coordinates for the first narrowband pair of filters (H α 1 and H α 2) in our survey, where the red vertical line represents a RA=0°. The Individual colored boxes represent one pointing with a 7.26 deg 2 field of view. The color bar indicates how many observations have been taken for each pointing

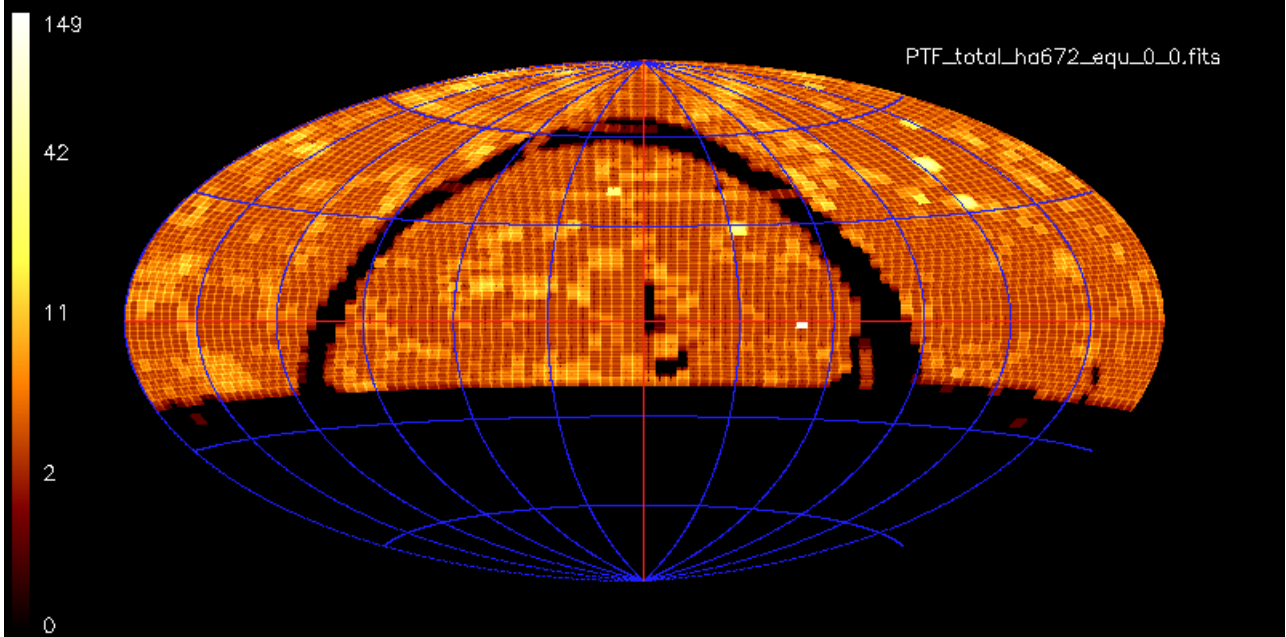


Figure 3. The sky coverage map in equatorial coordinates similar to Figure reffig:skymap1 but for the second narrowband pair of filters (H α 3 and H α 4) in our survey. The dark contiguous sections represents the Galactic plane which is avoided in the second filter pair.

2.5 Ancillary Data

We supplement our CLU-H α fluxes with information from the SDSS DR12 (Alam et al. 2015), GALEX all sky (Martin et al. 2005), and WISE all sky surveys (Wright et al. 2010) in addition to PS1 PSF and Kron magnitudes. We utilize the model *ugriz* magnitudes from SDSS DR12. In addition, we cross-match the CLU-H α sources against entries in the SDSS ‘galSpecLine’ table and extract the redshift, H α line flux

(‘h_alpha_flux’), and equivalent width (EW; ‘h_alpha_eqw’). We also extract FUV and NUV kron fluxes from the GALEX all-sky imaging survey (AIS; Bianchi, Conti & Shiao 2014), and the instrumental profile-fit photometry of the first and fourth WISE bands (‘w1mp’ and ‘w4mp’). These ancillary data are used to cull contaminants and measure several physical properties of galaxies.

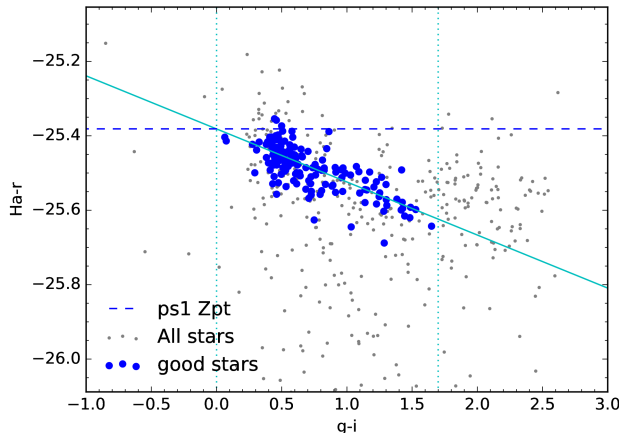


Figure 4. The Ha-r versus g-i color plot which is used to define our photometric calibration (i.e., zeropoint and color correction). The blue filled points are all stars selected for calibration, the horizontal blue line represents the zeropoint, and the solid cyan line is the fit to calibrations stars and is used for color corrections.

3 CANDIDATE SELECTION

In this section, we describe our galaxy candidate selection methods. We have chosen to test these methods in 14 preliminary fields that have SDSS coverage which contain many galaxies with existing spectroscopic redshifts. Furthermore, we have obtained spectra for all remaining candidates, thus facilitating a robust estimation of the success, false-positive, and false-negative rates of our selection criteria.

3.1 Preliminary Fields

The preliminary fields were chosen based on the following criteria: 1) the CLU-H α images must contain H α filter pairs taken on the same night and have observations in all four filters to ensure a complete analysis, 2) the field must have SDSS coverage to provide a list of galaxies with known redshifts, and 3) a declination close to 30° to facilitate spectroscopic follow-up from Palomar Observatory. These three criteria will allow us to generate galaxy candidates, test our selection methods, and accurately describe the success rates and limits of our survey. The basic properties of the 14 preliminary fields are listed in Table 4.

In addition, we have chosen to include one field which contains a galaxy cluster. The field labeled “p3967” in Table 4 is spatially coincident with the Coma cluster whose redshift falls in the wavelength range of our third narrow-band filter (H α 3). Since the population of any galaxy cluster is dominated by “red-and-dead” galaxies with little-to-no star formation (i.e., low H α equivalent widths), this field represents a worst case scenario for our selection methods. We include this field to robustly test the limits of our selection methods. However, the majority of the preliminary fields occupy relatively sparse sections of the sky (i.e., outside the Galactic plane and not coincident with any galaxy clusters). Each pointing in our H α survey covers 7.26 deg^2 on the sky; thus our 14 preliminary fields cover a total of 101.6 deg^2 .

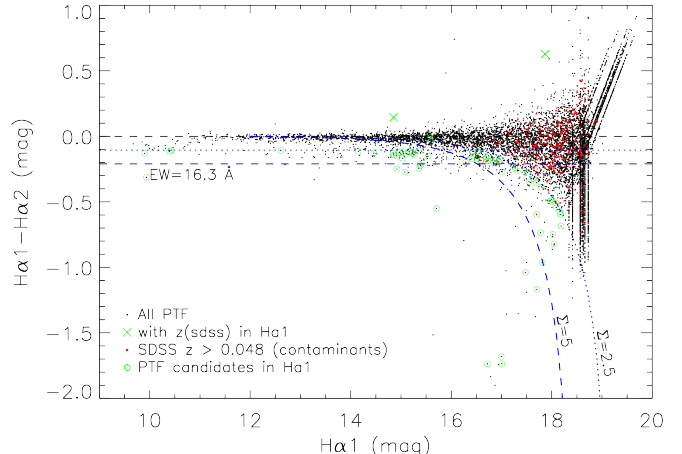


Figure 5. The H α color-magnitude diagram used for identification of emission-line sources in the H α 1 filter, where the y-axis represents the “On-Off” color and the x-axis is the “On” magnitude. The black points represent all CLU-H α sources, the red dots represent contaminant galaxies with $z > 0.048$, the green X’s represent known galaxies with a redshift that fall in the wavelength range of the H α 1 filter, and the green circles represent the galaxy candidates selected. The dotted and dashed lines represent the Σ cuts of 2.5 and 5, respectively. The “On-Off” color defined by the standard deviation of bright stars is converted into an H α EW limit and is labeled for the $\Sigma = 5$ cut (horizontal dashed line) with a value of 16.3 \AA .

3.2 Candidate Selection Criteria

The identification of emission-line candidates follows the general methods of previous emission-line galaxy surveys (e.g., Bunker et al. 1995; Pascual et al. 2001; Fujita et al. 2003; Sobral et al. 2009; Ly et al. 2010; Lee et al. 2012; Stroe & Sobral 2015). The photometry used for the selection process are taken from the Source Extractor catalogs. We use the 5 pixel diameter aperture photometry for all selection criteria. In addition, we require a candidate to have a 5σ detection in the “On” band and set non detections to the 5σ upper limit (see Table 4).

Emission-line candidates are selected based on the significance of the excess in “On-Off” color, where the flux is greater in one filter (the “On” filter) due to the presence of an emission line compared to the corresponding continuum filter (the “Off” filter). Each filter pair (H α 1/H α 2 and H α 3/H α 4) provides both the “On” and “Off” photometry. For example, H α 2 is used as the “Off” filter for H α 1 selection, while H α 1 is used as the “Off” filter for H α 2 selection.

We employ two selection criteria to identify true H α color excess sources: 1) the standard deviation of “On-Off” colors of bright continuum sources with magnitudes between 12 and 15 mag, and 2) a standard signal-to-noise selection (e.g., Sobral et al. 2009; Stroe & Sobral 2015) in which the noise in each image pair is added in quadrature via:

$$\delta = \sqrt{\pi r^2(\sigma_{\text{on}}^2 + \sigma_{\text{off}}^2)}, \quad (3)$$

where $\sigma_{\text{on/off}}$ represent the median sky count fluctuations in 100 sky regions for the “On” and “Off” images. We use

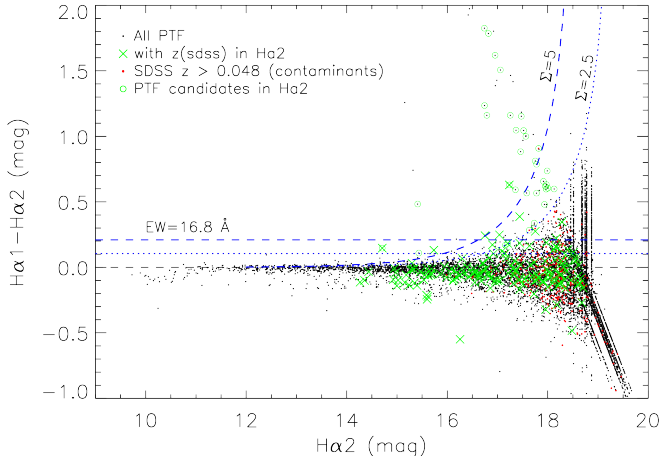


Figure 6. The H α color-magnitude diagram used for emission-line sources in the H α 2 filter similar to that in Figure 5. The “On-Off” color defined by the standard deviation of bright stars is converted into an H α EW limit and is labeled for the $\Sigma = 5$ (horizontal dashed line) with a value of 16.8 Å.

the parameter Σ to quantify the significance of the color excess above these two color quantities (i.e., that of random scatter), where the relationship between “On-Off” color, δ , and Σ is given by:

$$m_{\text{off}} - m_{\text{on}} = -2.5 \log(1 - \Sigma \delta 10^{-0.4(ZP - m_{\text{on}})}) \quad (4)$$

where $m_{\text{on/off}}$ are the calibrated magnitudes in the “On” and “Off” filters and ZP is the photometric zero-point for the “On” filter.

We utilize two Σ cuts to define the extremes of our candidate selection methods. The first is a cut of $\Sigma = 2.5$ which will contain the majority of all star-forming galaxies but will contain a relatively higher contamination fraction of high-z galaxies. The second is a cut of $\Sigma = 5$ which will contain a reduced fraction of all star-forming galaxies but will contain a low contamination fraction (see § 4.4).

These cuts are graphically presented on the color-magnitude diagrams in Figures 5–8 for each H α filter in one PTF field (“p3967”). In each of these figures the black points represent all CLU-H α sources, the red dots represent known galaxies with a spectroscopic redshift greater than our filter’s wavelength coverage ($z > 0.048$), the green X’s represent known galaxies with a spectroscopic redshift that fall in the wavelength range of the appropriate filter, and the green circles represent the galaxy candidates selected in each filter.

The color excess cut based on bright continuum sources represents the minimum color at all magnitudes below which we cannot accurately infer the presence of an emission line (e.g., H α). Furthermore, since the EW of an emission line is simply the ratio of the line flux and the continuum flux density, we can calculate an EW limit based on the “On-Off” color scatter in bright continuum sources. Following the prescription of (Stroe & Sobral 2015, see Equation 7), the EW can be calculated via:

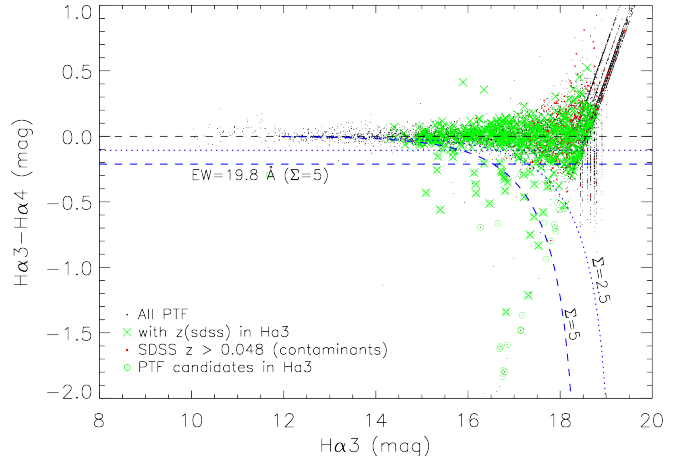


Figure 7. The H α color-magnitude diagram used for emission-line sources in the H α 3 filter similar to that in Figure 5. The overabundance of galaxies for this filter is due to the Coma cluster which is dominated by early type galaxies with little on-going star formation. The lack of star formation in these galaxies is evident from the lack of significant H α “On-Off” colors. The “On-Off” color defined by the standard deviation of bright stars is converted into an H α EW limit and is labeled for the $\Sigma = 5$ cut (horizontal dashed line) with a value of 19.8 Å.

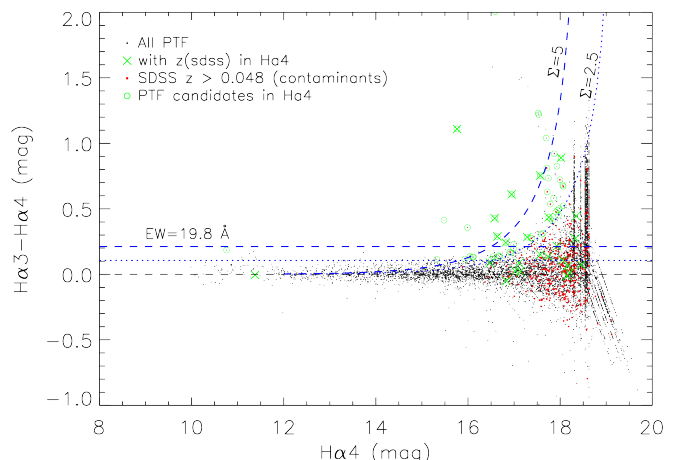


Figure 8. The H α color-magnitude diagram used for emission-line sources in the H α 4 filter similar to that in Figure 5. The “On-Off” color defined by the standard deviation of bright stars is converted into an H α EW limit and is labeled for the $\Sigma = 5$ cut (horizontal dashed line) with a value of 19.8 Å.

$$\text{EW} = \Delta\lambda_{\text{On}} (10^{-0.4\Delta m} - 1), \quad (5)$$

where $\Delta\lambda_{\text{On}}$ is the FWHM of the “On” filter and Δm is the “On-Off” color. The EW cuts based on the “On-Off” colors for each filter in Figures 5–8 are labeled on the horizontal dashed and dotted lines for $\Sigma = 2.5$ and $\Sigma = 5$, respectively. The median EW cut and standard deviation for all filters in the 14 preliminary fields is 7.3 ± 1.1 Å and 15.2 ± 2.4 Å for $\Sigma = 2.5$ and $\Sigma = 5$, respectively.

3.3 Contaminant Removal

The two color excess cuts introduced in the last section will effectively select any source that has a significant H α “On-Off” color. However, the resulting galaxy candidates can still be contaminated by continuum sources with steep blue or red continuum slopes, high-redshift galaxies with an emission or absorption line whose wavelength has been redshifted into the wavelength range spanned by one of our filters, and cosmic rays or chip defects (e.g., hot pixels, column defects, etc.).

Point sources with a steep blue or red continuum can be reduced by requiring that our candidates be spatially extended. As our survey is only sensitive to a distance of 200 Mpc and our angular resolution is limited to a FWHM $\sim 2''$, we estimate that galaxies larger than 2 kpc at 200 Mpc will be extended in our data. Comparison to a statistically complete sample of star-forming galaxies in the local Universe where the sample is dominated by dwarf galaxies (LVL; Kennicutt et al. 2008; Dale et al. 2009; Lee et al. 2011; Cook et al. 2014a) reveals that the semi-major axis histogram peaks between 2 – 4 kpc suggesting that we will likely detect the majority of galaxies even at our furthest distance by requiring our galaxy candidates to be extended. Similar results are found for the size of H α disks in galaxies out to $z=0.1$ (Dale et al. 1999). We exclude point sources based upon the recommended PS1 star/galaxy separation using PSF minus Kron i-band magnitudes.

Unfortunately, the PS1 star-galaxy classifications often mislabel saturated stars as galaxies at r-band magnitudes brighter than 12-14 mag⁷ leaving ~ 300 candidates that are clearly stars. We can remove $\sim 60\%$ of these contaminants via a bright H α magnitude cut of 12 mag given the brightest quoted saturation magnitude in PS1. We note that the brightest confirmed galaxy in the preliminary fields is ~ 13.4 mag. The remaining contamination stars are removed via visual classification.

Another source of contamination stems from cosmic rays and chip defects. The removal of these contaminants is achieved by requiring a source to be spatially coincident with a PS1 source. Since the PS1 detection limits (e.g., $r \sim 23.2$ mag) are deeper than the CLU-H α single-image exposures, any cosmic ray or chip defect with no spatial overlap with a PS1 source will be easy to flag and remove. Visual inspection of sources removed from our analysis via this method show that no real sources have been removed. Furthermore, visual inspection of our galaxy candidates show no contamination from cosmic rays, but do show a small percentage of contamination from chip-column defects that randomly coincide with a PS1 source; these contaminants are easily removed via visual inspection, and will be greatly reduced after stacking images for the entire survey.

The final source of contamination is high redshift galaxies whose emission or absorption lines have been shifted into the wavelength range of our filters. It will not be possible to distinguish between strong emission lines redshifted into the wavelength range of our filters and H α emission at lower redshift. We note that there is a dearth of strong emission lines blue-ward of our filters the closest being the

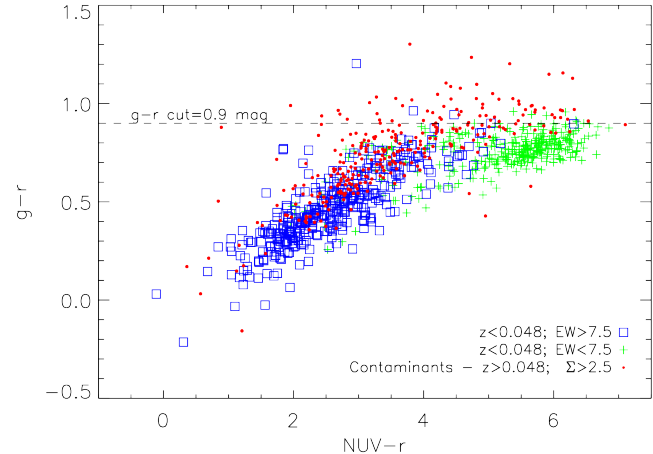


Figure 9. The g-r versus NUV-r, color-color plot of all known galaxies in the preliminary fields, where the blue squares represent galaxies in our target volume with an H α EW greater than the $\Sigma = 2.5$ limit ($EW \geq 7.5 \text{ \AA}$), the green pluses are all galaxies in our volume with small H α EWs ($EW < 7.5$), and the red points are galaxy candidates outside of our target volume ($z > 0.048$). A g-r optical color cut removes contaminant galaxies while retaining the majority of galaxies in our volume with an EW greater than our selection limits ($EW \geq 7.5 \text{ \AA}$).

[OIII] $\lambda 4959, \lambda 5007$ doublet near $\lambda = 5000 \text{ \AA}$ ($z \sim 0.3$). However, galaxies with extreme [OIII] $\lambda 4959, \lambda 5007$ emission at $z \sim 0.3$ are likely to be interesting objects (i.e., green peas) and can be used for studies of galaxy evolution and star formation. In fact, we find a newly discovered $z \sim 0.3$ green pea contaminant in the preliminary fields (see § 5.1) and future CLU efforts will be aimed at studying these objects.

Contamination from redshifted absorption line sources, on the other hand, can be removed via optical color cuts. Many studies have found a dichotomy in the optical and UV colors of star-forming galaxies and those with little-to-no star formation (e.g., red sequence galaxies; Salim et al. 2007). SDSS studies have shown that red sequence galaxies exhibit optical g-r colors greater than 0.8 ± 0.1 mag and that star-forming galaxies show g-r less than 0.8 mag. Figure 9 shows the g-r versus NUV-r color-color diagram for all galaxies with H α EW measurements (SDSS and CLU-H α follow-up) that are found in the footprint of the 14 preliminary fields. The blue boxes represent $z < 0.048$ galaxies with an H α EW larger than 7.5 \AA (i.e., the EW limit for $\Sigma = 2.5$ sample), the green pluses represent $z < 0.048$ galaxies with an H α EW smaller than 7.5 \AA , and the red dots represent high redshift contaminants ($z > 0.048$) with a color significance greater than 2.5 mag ($\Sigma > 2.5$). We find that a g-r color cut (horizontal dashed line) removes 60% of high-z candidates (red dots) while removing only 4 galaxies with moderate EW and a redshift less than 0.048. We use a cut of g-r greater than 0.9 mag to remove any galaxies with little star formation whose H α emission line will be effectively undetectable by our methods.

⁷ <https://panstarrs.stsci.edu/>

3.4 Spectroscopic Follow-up

We have obtained spectra for all candidates with no redshift information (except obvious stars, cosmic rays, and chip defects) with a Σ value above 2.5. The spectra were taken on the 200 inch Hale telescope atop Palomar Mountain on multiple nights over 2016 and 2017 using the Double-Beam Spectrograph instrument (DBSP; Oke & Gunn 1982) and on the 2.3 meter Wyoming Infra-Red Observatory (WIRO) with the Longslit spectrograph. The DBSP data were reduced using the PyRAF-based pipeline⁸ of Bellm & Sesar (2016) and the WIRO data were reduced with standard IRAF procedures.

We took spectra of 334 galaxies where we confirm that 124 galaxies were indeed galaxies with redshifts less than 0.048, while the remainder were higher-redshift contaminants. In addition to finding new galaxies in the target volume, we also found 2 new galaxies (QSO and green pea) at intermediate redshift via strong [OIII] λ 4959, λ 5007 emission lines redshifted into our filters (see § 5.1).

3.5 Photometric H α Fluxes

Since the majority of galaxies in the full $\approx 3\pi$ area of the CLU-H α survey will not have spectroscopic H α fluxes it is necessary to confirm that the photometric fluxes measured in our survey agree with those derived from spectroscopic measurements. In Figure 10 we plot the photometric H α line flux versus the spectroscopic line flux in the left panel. The photometric H α line flux is measured via:

$$F_{\text{line}}(\text{erg/s/cm}^2) = \Delta\lambda_{\text{On}}(f_{\text{On}} - f_{\text{Off}}), \quad (6)$$

where $\Delta\lambda_{\text{On}}$ is the FWHM of the “On” filter, f_{On} is the flux density of the “On” filter, and f_{Off} is the flux density of the “Off” filter. The flux densities of the “On” and “Off” filters are calculated via:

$$f_{\text{on,off}}(\text{erg/s/cm}^2/\text{\AA}) = \frac{c}{\lambda_{\text{on,off}}^2} 10^{-0.4(m_{\text{on,off}} + Z_{\text{PTAB}})}, \quad (7)$$

where c is the speed of light, $Z_{\text{PTAB}} = 48.59$, and $\lambda_{\text{on,off}}$ are the central wavelengths of the “On” and “Off” filters.

There is good agreement for the majority of galaxies above a few $\times 10^{-15}$ erg/s/cm² for line fluxes derived from our H α photometry and those derived from spectroscopy. However, there is disagreement at fluxes below 1×10^{-15} erg/s/cm² where the photometrically derived fluxes are systematically higher than the spectroscopic fluxes. This floor in the photometrically-derived fluxes represent an effective H α line flux limit and is a consequence of our selection criteria, where the “On” flux must be brighter by some Σ threshold above the “Off” flux and the “Off” flux is limited to the 5σ detection threshold of the image. In other words, at fainter “On” fluxes the corresponding “Off” flux will approach the detection limit of the image thus limiting the resulting line flux to Σ above the “Off” flux. This line flux limit will vary for different $\Sigma = 2.5$ and $\Sigma = 5$ galaxy catalogs since the Σ threshold represents an “On-Off” color (i.e., a line flux).

To quantify the limit imposed by our selection criteria we take the minimum photometrically derived H α line flux for both $\Sigma = 2.5$ and $\Sigma = 5$ galaxy catalogs. The limits are 2 and 4×10^{-15} erg/s/cm² and are represented as dotted- and dashed-horizontal lines in Figure 10 for $\Sigma = 2.5$ and $\Sigma = 5$, respectively. Assuming the median 5σ detection limit for all images of ~ 18.5 mag, we can estimate the apparent magnitude limits for the “On” filter of both galaxy catalogs using Equations 7 and 6. The apparent narrowband magnitude limits are 18.3 and 18.0 for the $\Sigma = 2.5$ and $\Sigma = 5$, respectively.

4 RESULTS

In this section we provide a description of the CLU-H α galaxies found in the preliminary fields and highlight two sub-samples composed of: 1) galaxy candidates with lower color significance ($\Sigma \geq 2.5$) that will contain the majority of target galaxies but with high contamination; 2) galaxy candidates with higher color significance ($\Sigma \geq 5$) that contain a reduced fraction of target galaxies but with low contamination. First, we present examples of newly discovered galaxies in the H α survey. Then, we examine the observable properties of the galaxies in our CLU-H α catalog and derive their physical properties. Next, we compare the list of CLU-H α galaxies to all known galaxies in the preliminary fields and evaluate the success rates of our selection methods. Furthermore, we quantify the limits of the H α survey and use these limits to estimate our completeness as compared to a statistically complete sample of nearby galaxies. Finally, we compare the CLU-H α galaxies found in the preliminary fields to a compiled catalog of all known galaxies in the local Universe, the CLU-compiled catalog.

We note that the H α galaxy catalogs and analyses presented here utilize single exposure images; not the final stacked images. The stacked CLU-H α images will produce a galaxy catalog with fainter detection limits, higher success rates, and a higher completeness than the preliminary fields presented here. The stacking methods and analysis of the CLU-H α images is the subject of a future study and beyond the scope of this paper.

4.1 Example New Galaxies

Here we present examples of CLU-H α galaxies with no previous distance information that are now well constrained to be in the local Universe. Figure 11 presents a mosaic of a representative sample of newly discovered galaxies (i.e., galaxies with no previous redshift) found in the correct filter, where the left image cutout is the SDSS gri color composite, the four panels to the right are the cutouts for all four H α filters, and the green boxes highlight which filter the source is identified (i.e., the brightest). The galaxies in this mosaic span the range of H α EW, where EW increase towards the bottom of the figure from EW=10 Å at the top to EW=100 Å at the bottom. The galaxies also show a range of morphologies from compact to irregular to those showing spiral structure.

⁸ <https://github.com/ebellm/pyraf-dbsp>

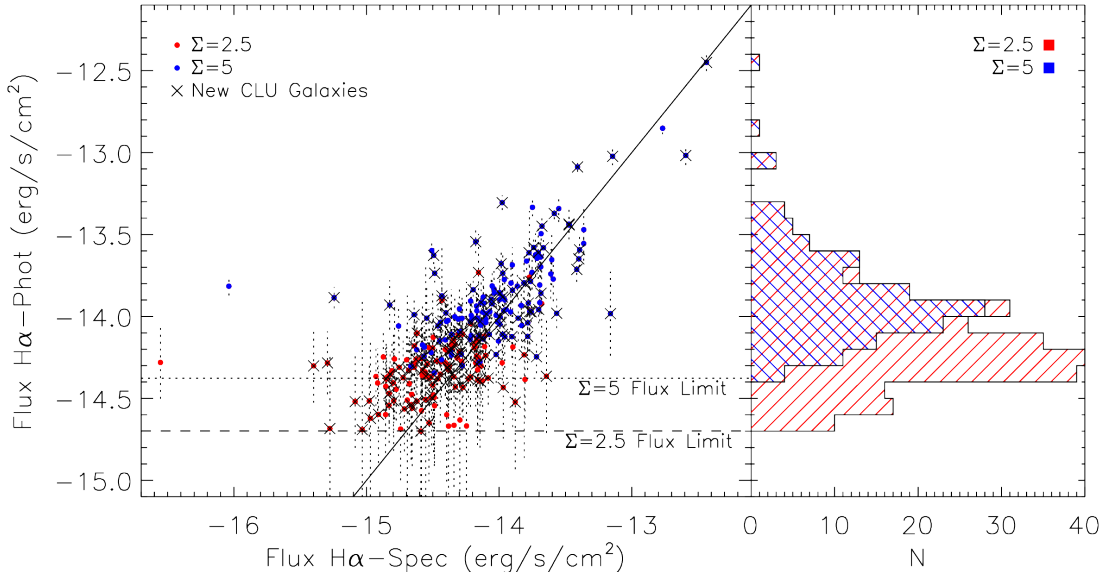


Figure 10. Left Panel) The photometrically-derived H α line flux versus the spectroscopically-derived H α line flux in the left panel. We find that the majority of the galaxies show good agreement for H α line fluxes between those derived from imaging and spectroscopy above a few $\times 10^{-15}$ erg/s/cm 2 . Right Panel) The histogram of the $\Sigma = 2.5$ and $\Sigma = 5$ CLU-H α galaxy samples showing the minimum H α flux derived from imaging. These lower flux values represent a selection limit that stem from the 5σ detection limit in the “Off” filter. The flux limits imposed by our selection limits for the $\Sigma = 2.5$ and $\Sigma = 5$ CLU-H α galaxy samples translate to an H α “On” magnitude limit of 18.3 and 18.0 mag, respectively.

4.2 Observable Properties of CLU-H α Galaxies

Here we examine the composition and galaxy properties of our H α galaxy catalog in the preliminary fields (i.e., $\Sigma \geq 2.5$). We explore the SDSS g-r color, apparent SDSS r-band magnitude, the absolute r-band magnitude, and the H α luminosity of the $\Sigma = 2.5$ galaxy candidates in Figure 12. In all panels of Figure 12 the black-open, red-diagonal filled, and blue-diagonal filled histograms represent all known galaxies in our fields, all galaxies with an H α EW greater than 7.5 Å, and our confirmed galaxy candidates with an H α EW greater than 7.5 Å, respectively. We do not show the observable properties for $\Sigma = 5$ catalog since their distributions are similar to the $\Sigma = 2.5$ catalog.

Panel ‘a’ of Figure 12 shows the SDSS g-r histogram where the majority of all galaxies show a g-r color around 0.8 mag and is consistent with an overabundance of elliptical galaxies. This is expected since one of our pointings cover the Coma cluster which is dominated by ellipticals (see § 3.1). Both subsets of all galaxies with greater H α EWs tend to have bluer g-r colors where the candidate galaxies show a similar distribution of optical colors. Thus, our selection methods are not biased in optical color when compared to galaxies with moderate H α EWs, but are biased towards blue colors when compared to all galaxies.

Panel ‘b’ of Figure 12 shows the apparent r-band magnitude where all three histograms shows similar distributions. However, the histogram for all galaxies with EW>7.5 is peaked at fainter magnitudes than the histogram for the galaxy candidates suggesting that the galaxies with moderate EWs missed in our survey are the fainter ones near 18th mag.

Panel ‘c’ of Figure 12 shows the absolute r-band magnitude where all three histograms show similar distributions. However, there is a small overabundance of intrinsically bright galaxies which is likely the result of an overabundance of elliptical galaxies with red optical colors that tend to be more massive (i.e., brighter). Comparison of both subsets with EW>7.5 reveal that both histograms span the same absolute magnitude range; however, a fraction of the galaxies missed in our catalog tend to be the intrinsically faint galaxies. The likely explanation for this is that our catalog has missed intrinsically faint galaxies that are farther away, and thus, are harder to detect due to larger photometric uncertainties.

Panel ‘d’ of Figure 12 shows the H α luminosity where the two galaxy subsets with EW>7.5 Å tend to have higher luminosities compared to all galaxies. This panel clearly illustrates that a large fraction (>50%) of all galaxies in our fields are intrinsically faint in H α emission (i.e., small H α EWs). A comparison between the two subsets of galaxies with EW>7.5 shows that our galaxy candidates have a similar luminosity peak as all galaxies with EW>7.5, but tend to occupy the higher luminosity side of the distribution.

4.3 Physical Galaxy Properties

Here we present the physical properties of the galaxy sample by cross-matching against the ALLWISE 3.4 and 22 μ m fluxes. These data will provide stellar mass (M_*) and extinction corrections due to dust. In addition, we use the spectroscopic H α fluxes of our survey to measure H α -derived SFRs. The H α fluxes have been corrected for Milky Way extinction via the prescription of Schlafly & Finkbeiner (2011).

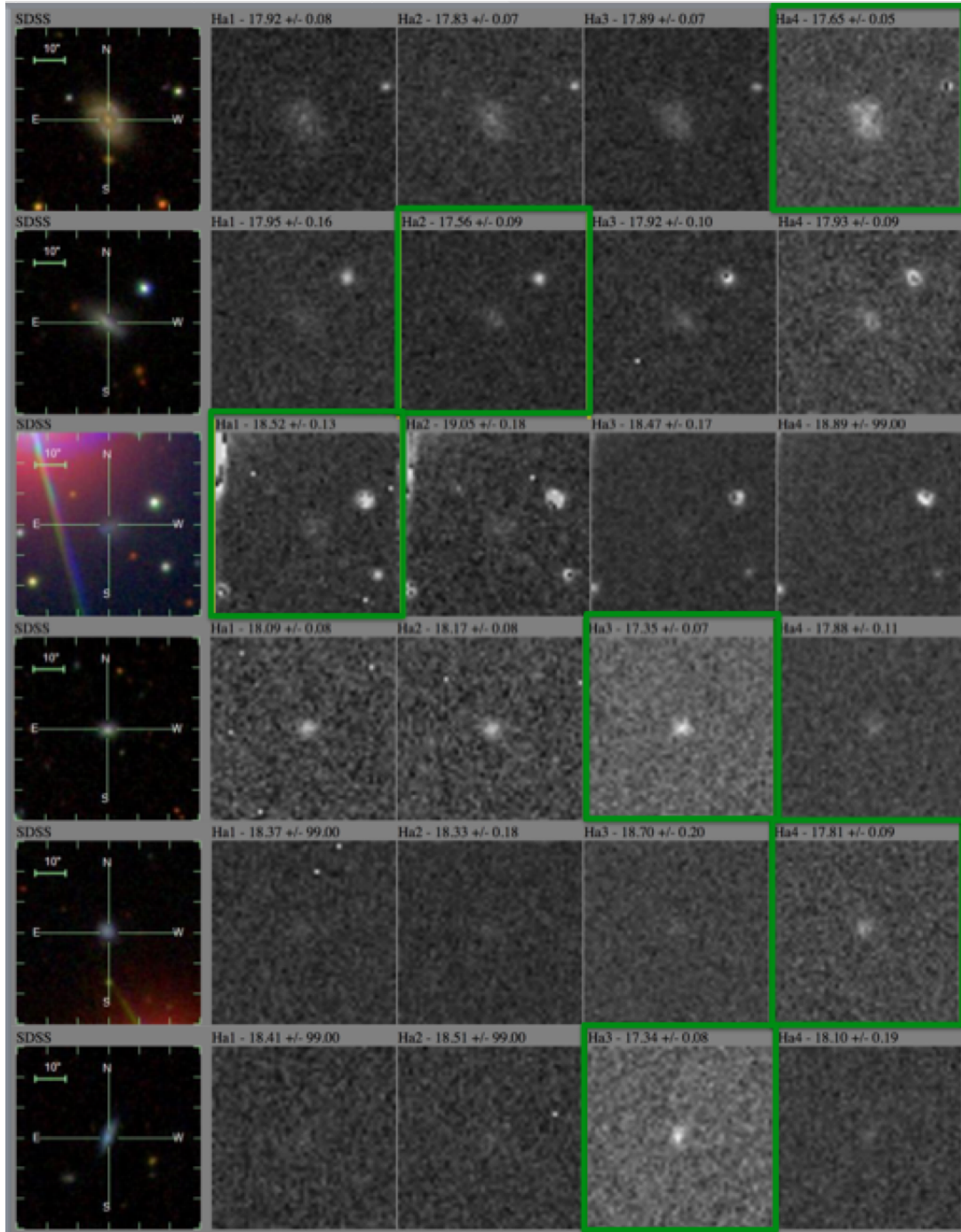


Figure 11. A mosaic of a representative sample of newly discovered galaxies in the local Universe, where (from left-to-right) the image cutouts are the SDSS gri composite and followed by the four H α filters (H α 1-H α 4). The H α magnitudes and errors are listed above each H α cutout and the green boxes indicate which filter the galaxy was identified (i.e., the brightest). In addition, the galaxies are sorted by H α EW, where the lowest EW galaxies are at the top (EW~10 Å) and the highest are at the bottom (EW~100 Å).

The stellar masses are derived from mass-to-light ratios (Υ_*) using the WISE 3.4 μ m fluxes. We utilize the fluxes derived from ALLWISE catalog profile fitting photometry, thus these fluxes should encompass each galaxies' full radial extent. The WISE 3.4 μ m bandpasses provides a robust tracer of a galaxy's stellar mass as this light is dominated by an older stellar population (which make up the majority

of a galaxy's stellar mass) and is less affected by attenuation from dust than shorter wavelengths.

Many studies over the past few years have made comparisons between a variety of observationally derived stellar masses (e.g., baryonic Tully-Fisher relationship and resolved star color-magnitude diagrams) and luminosities in Spitzer 3.6 μ m and WISE 3.4 μ m bandpasses (Oh et al. 2008; Es-

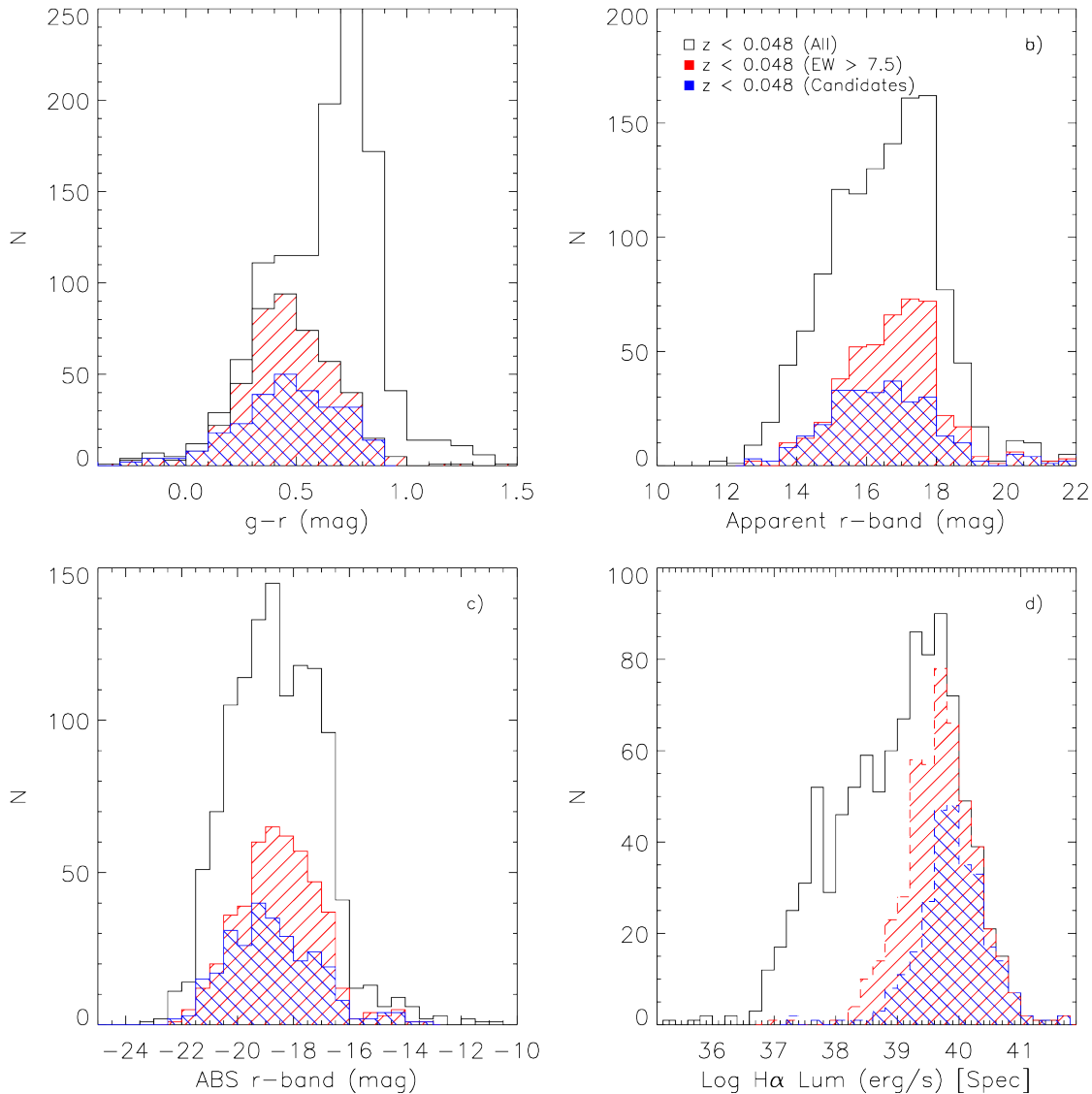


Figure 12. The observable property histograms of galaxies in the local Universe where unfilled, blue-filled, and red-filled histograms represent all galaxies in our volume, all galaxies in our volume with an $\text{EW} > 7.5 \text{ \AA}$, and all $\Sigma = 2.5$ candidates, respectively. Panel a) shows the $g-r$ optical colors, panel b) shows the apparent r-band magnitudes, panel c) shows the absolute r-band magnitudes, and panel d) shows the $\text{H}\alpha$ derived luminosities. We find that our candidates are not biased with respect to the known local Universe galaxies with an EW greater than our selection limit.

kew, Zaritsky & Meidt 2012; Barnes et al. 2014; McGaugh & Schombert 2014; Meidt et al. 2014; Norris et al. 2014; McGaugh & Schombert 2015; Querejeta et al. 2015). The results of these comparisons show that a constant Spitzer $\Upsilon_{*}^{3.6\mu\text{m}}$ of $0.4 - 0.55$ provides a robust estimation of a galaxies stellar mass with a relatively low error of ~ 0.1 dex (Meidt et al. 2014; McGaugh & Schombert 2015). A constant mass-to-light ratio of the same value for WISE $3.4\mu\text{m}$ has been shown to yield similar stellar masses as Spitzer $3.6\mu\text{m}$ (Jarrett et al. 2013; Norris et al. 2014). We adopt the constant mass-to-light ratio of $\Upsilon_{*}^{3.4\mu\text{m}} = 0.5 \text{ M}_{\odot}/\text{L}_{\odot,3.4\mu\text{m}}$, where $\text{M}_{\odot}/\text{L}_{\odot,3.4\mu\text{m}}$ is the mass-to-light ratio in units of solar masses per the solar luminosity in the WISE $3.4\mu\text{m}$ filter bandpass ($\text{m}_{\odot,3.4\mu\text{m}} = 3.24 \text{ mag}$; $\text{L}_{\odot,3.4\mu\text{m}} = 1.58 \times 10^{32} \text{ erg s}^{-1}$; Jarrett et al. 2013).

Star formation rates (SFRs) for our galaxies can be estimated from many different luminosity tracers (e.g. $\text{H}\alpha$, FUV, etc.), where measured luminosities are transformed into SFRs via scaling prescriptions (e.g., Kennicutt 1998; Murphy et al. 2011). We utilize the updated scaling relationships of Murphy et al. (2011) which assumes a Kroupa IMF (Kroupa 2001). The $\text{H}\alpha$ SFRs are derived via a combination of $\text{H}\alpha$ and $22\mu\text{m}$ luminosities which account for internal dust extinction (Calzetti et al. 2010; Murphy et al. 2011):

$$\text{SFR}_{\text{H}\alpha,\text{corr}}(\text{M}_{\odot}\text{yr}^{-1}) = C \times \nu L_{\text{H}\alpha} + 0.031 \times \nu L_{22\mu\text{m}}, \quad (8)$$

where νL are the observed monochromatic luminosities of both $\text{H}\alpha$ and the WISE4 band at $22\mu\text{m}$ in ergs per second and $C = 5.37 \times 10^{-42}$ (Murphy et al. 2011).

The two panels of Figure 13 show the H α -derived SFRs and stellar masses for all known galaxies in our preliminary fields, all galaxies with an H α EW > 7.5 Å, and the CLU-H α galaxies (i.e., $\Sigma > 2.5$). Panel a) shows the SFR histograms where both subset galaxies with EW > 7.5 Å tend to occupy the high SFR end of all known galaxies. In addition, the CLU-H α galaxies span the same range as the subset of all galaxies with an EW > 7.5 Å. Panel b) of Figure 13 shows the stellar mass histograms where all three samples show the same M_* distribution. However, the CLU-H α galaxies are peaked at the higher mass end of the relatively “top-hat” distribution of all galaxies and all galaxies with an EW > 7.5 Å.

4.4 Comparison to Known Galaxies

We examine the candidate composition at various Σ cuts, and evaluate the robustness of our selection criteria via a comparison between our galaxy candidates and all known galaxies with a spectroscopic redshift in the preliminary fields. Given that our selection methods rely on the presence of a moderately strong H α emission line, we expect that we should recover a large fraction of the H α flux for all galaxies but a relatively low fraction of the number of all galaxies due to the numerous early type galaxies in these fields (>50%).

First, we evaluate which color excess significance (Σ) value yields the maximum number of galaxies in the target redshift range while minimizing the number of stars (those not removed by automated star/galaxy classification) and high-z galaxy contaminants. We remove cosmic rays and chip defects from this analysis since these contaminants will be cleaned in the stacked images used by future studies. In this experiment, we use Σ cuts of 2.5, 3, 4, 5, 6, and 7 mag. The total number of candidates, contaminant stars, contaminant high-z galaxies, galaxies found in the volume ($z < 0.048$), galaxies found in the correct filter, and newly discovered galaxies found in the correct filter are presented in Table 2.

We find that as the color significance Σ increases, the total number of candidates, contaminants, and galaxies found in the correct filter decreases. Furthermore, the percentage of high-z contaminants decreases towards higher Σ values, where the contamination percentage drops steeply above $\Sigma = 3$ then levels off to a few percent at $\Sigma = 5$. The percentage of galaxies found in the correct filter, on the other hand, increases at higher Σ values, where the percentage increases steeply at low Σ values and levels off $\geq 75\%$ at $\Sigma = 5$. We conclude that $\Sigma = 2.5$ produces a catalog with more galaxies in our volume but higher contamination while $\Sigma = 5$ produces a high fidelity galaxy catalog where the majority of candidates are galaxies found in the correct filter with little contamination. We focus the text in the rest of this section on the two extreme galaxy catalogs ($\Sigma = 2.5$ and $\Sigma = 5$) but provide the statistics for all Σ cuts in the tables.

Next we quantify the success rates of the resulting galaxy catalogs at various Σ values. The simplest comparison we can make is to that of the number of galaxies found in our analysis to all known galaxies in the same sky coverage regardless of the strength of the H α line (i.e., H α EW). The results of this comparison are presented in Table 3 for

the different Σ values studied here. Of the known galaxies, we successfully recover 24.2% and 12.4% by number for Σ cuts of 2.5 and 5, respectively (see column 2 in Table 3).

However, these estimates are not an accurate description of our success rate since our detection method relies on the presence of an H α emission line. Thus, galaxies with low H α EWs (i.e., low SFR activity) in our preliminary fields will bias our success rates to lower values. There are 1226 known galaxies in our preliminary fields with a redshift in our filters’ wavelength range. The number of known galaxies with H α EWs lower than 7.5 Å is 722 ($\approx 60\%$), of which 465 are located in a single pointing that is coincident with the Coma cluster (i.e., ‘p3967’). Thus our inclusion of this pointing has biased our success rate by number to low values.

Another way to quantify our success rate is to examine what fraction of H α flux is captured by our selection methods compared to all galaxies. The fraction of the total H α flux captured by each of the Σ cuts are presented in Table 3, where we recover 80.9% and 66.4% for Σ cuts of 2.5 and 5, respectively (see column 3 in Table 3). Thus our selection methods recover a much larger fraction of the total H α flux than the total number of galaxies; over half of which are elliptical galaxies with low SFR activity.

If we limit the sample of known galaxies to those with an H α EW larger than the limits for the $\Sigma = 2.5$, the success rates by number and H α flux increase. The total number of galaxies with an H α EW greater than 7.5 Å decreases significantly to 504 with a corresponding total H α flux of 3.89×10^{-12} (erg/s/cm 2). The resulting success rates are 52.0% by number and 85.2% by H α flux for the $\Sigma = 2.5$ sample. The success rates of other Σ samples can be found in column 5 of Table 3).

Next, we examine why galaxies with an EW greater than 7.5 Å are not selected as candidates (i.e., our false-negative rate). The top panel of Figure 14 shows the H α “On” magnitude histogram and the bottom panel shows the errors of both the H α “On” and “Off” magnitudes added in quadrature versus the H α “On” magnitude. The red and blue histograms/symbols in Figure 14 represent galaxies with a $\Sigma \geq 2.5$ and a $\Sigma < 2.5$, respectively. The H α “On” magnitude histogram in the top panel shows that the galaxies with an EW greater than 7.5 Å that are not found as candidates tend to be fainter. Thus, the significance of the H α emission line is reduced by the increased photometric noise. Furthermore, the bottom panel shows that these same galaxies with a moderate H α EW and fainter magnitudes also tend to have higher combined errors in the “On” and “Off” filters. We conclude that these galaxies are missed due to marginal detections where the relatively larger errors for both the “On” and “Off” bands make it more difficult to accurately measure their photometry, thus accurately infer the presence of an emission line. We note that the photometric errors will be reduced in the final stacked CLU-H α images resulting in higher success rates in future analyses.

If we limit the sample of known galaxies to those with an H α EW > 7.5 Å and an H α “On” magnitude brighter than 18 mag, the success rates by number and H α flux increase. The success rates increase to 68.2% by number and 89.3% by H α flux for the $\Sigma = 2.5$ sample.

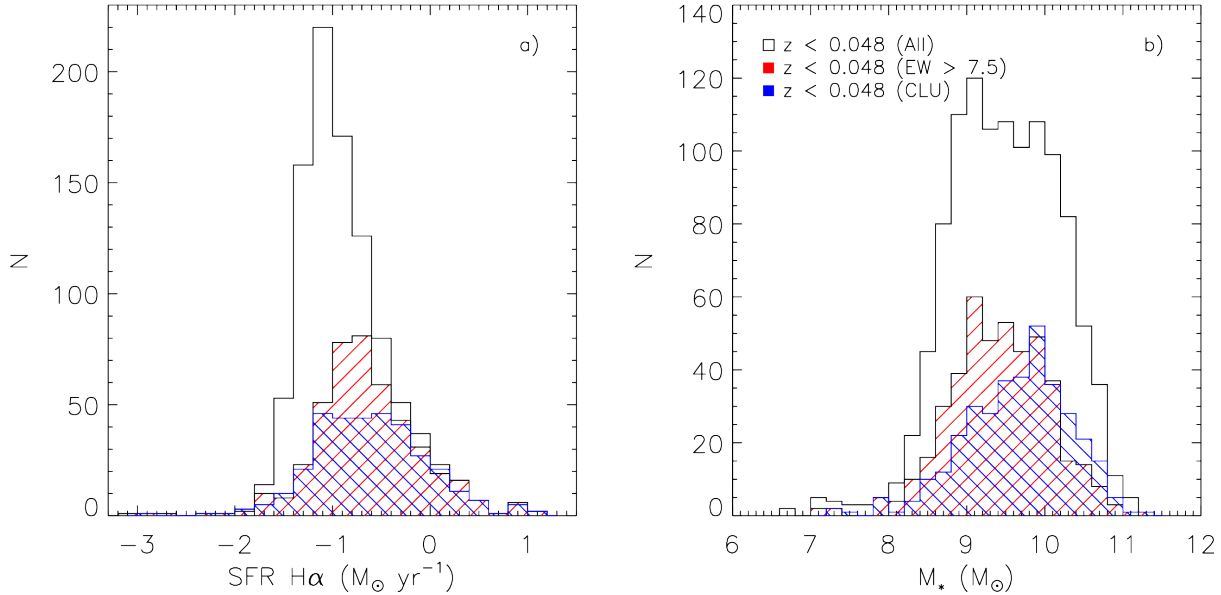


Figure 13. The physical property histograms of galaxies in the local Universe where unfilled, blue-filled, and red-filled histograms represent all galaxies in our volume, all galaxies in our volume with an $\text{EW} > 7.5 \text{ \AA}$, and all $\Sigma = 2.5$ candidates, respectively. Panel a) shows the $\text{H}\alpha$ derived SFRs and panel b) shows the stellar masses. We find that our candidates are not biased with respect to the known local Universe galaxies with an EW greater than our selection limit.

Color Excess (Σ) Statistics

Σ	N Total Candidates (#)	N Stars (#)	N High-z Galaxies (#, % of candidates)	N In Volume (#)	N in Correct $\text{H}\alpha$ Filter (#, % of candidates)	N New in Correct $\text{H}\alpha$ Filter (#)
≥ 2.5	793	82	317 (40.0%)	378	289 (36.4%)	89
≥ 3.0	497	53	134 (27.0%)	297	254 (51.1%)	77
≥ 4.0	282	25	39 (13.8%)	207	193 (68.4%)	55
≥ 5.0	197	14	14 (7.1%)	160	151 (76.6%)	40
≥ 6.0	150	12	7 (4.7%)	124	120 (80.0%)	31
≥ 7.0	124	9	3 (2.4%)	105	102 (82.3%)	22

Table 2. The composition of our galaxy candidates when using different Σ cuts, where the columns are from left-to-right: the minimum Σ for the sample, the total number of all candidates, the number of stellar contamination, the number high-redshift contamination, the number of galaxies found in the survey volume ($z < 0.048$), the number of galaxies whose $\text{H}\alpha$ emission-line is located in the narrowband filter where the galaxy was identified, and the number of galaxies newly discovered in the local Universe and found in the correct filter. We find that a $\Sigma = 5$ cut produces a catalog with the highest number of galaxies found in the correct filter while minimizing the high-z contamination.

4.5 Selection Limits

In this section we explore the limitations of our selection criteria and quantify them by magnitude and $\text{H}\alpha$ flux. We find that our magnitude limit is similar to, or slightly deeper, than the SDSS spectroscopic galaxy survey ($r \sim 18$ mag) and the 90% $\text{H}\alpha$ flux limit is $\sim 1 \times 10^{-14} \text{ erg/s/cm}^2$.

We first explore the distribution of absolute r-band magnitude and redshift for all known galaxies and CLU- $\text{H}\alpha$ galaxies in Figure 15, where the top panel presents the full redshift range while the bottom panel is a zoom-in of the local Universe ($z < 0.05$). The vertical dotted line represents the maximum redshift limit of our survey (i.e., $z = 0.048$), the dashed- and solid-curved lines represent the relationship between an apparent magnitude limit of 17.8

(i.e., the limit of the SDSS spectroscopic galaxy survey) and 19 mag, respectively, with redshift. The small black, larger red dots, larger blue dots, and X's represent all known galaxies, $\Sigma \geq 2.5$ CLU- $\text{H}\alpha$ galaxies, $\Sigma \geq 5$ CLU- $\text{H}\alpha$ galaxies, and CLU- $\text{H}\alpha$ galaxies with no previous distance information (i.e., newly discovered in the local Universe), respectively.

The density of known galaxies drops off significantly below the r-band magnitude limit of the SDSS spectroscopic galaxy survey ($r = 17.8$ mag). In addition, the density of CLU- $\text{H}\alpha$ galaxies also significantly decreases near or slightly deeper than that of SDSS suggesting that our selection methods result in an effect magnitude limit similar to the SDSS limit. However, we do find CLU- $\text{H}\alpha$ galaxies that are fainter than the SDSS limit, and that a large fraction of these galaxies are newly discovered to be in the local Uni-

Known Galaxies						
Sample	N (#) (no cut) (N,% of N)	Sum H α Flux (erg/s/cm 2) (no cut) (Flux,% of Flux)	N (#) (EW>7.5 Å) (N,% of N)	Sum H α Flux (erg/s/cm 2) (EW>7.5 Å) (Flux,% of Flux)	N (#) (EW>7.5 Å,mag<18) (N,% of N)	Sum H α Flux (erg/s/cm 2) (EW>7.5 Å,mag<18) (Flux,% of Flux)
All	1226	4.15e-12	504	3.89e-12	346	3.58e-12
$\Sigma \geq 2.5$	297 (24.2%)	3.36e-12 (80.9%)	262 (52.0%)	3.32e-12 (85.2%)	236 (68.2%)	3.19e-12 (89.3%)
≥ 3.0	261 (21.3%)	3.26e-12 (78.4%)	234 (46.4%)	3.22e-12 (82.7%)	216 (62.4%)	3.12e-12 (87.2%)
≥ 4.0	194 (15.8%)	2.96e-12 (71.1%)	181 (35.9%)	2.95e-12 (75.7%)	172 (49.7%)	2.88e-12 (80.5%)
≥ 5.0	152 (12.4%)	2.76e-12 (66.4%)	143 (28.4%)	2.75e-12 (70.7%)	139 (40.2%)	2.71e-12 (75.7%)
≥ 6.0	121 (9.9%)	2.57e-12 (61.9%)	113 (22.4%)	2.57e-12 (65.9%)	112 (32.4%)	2.55e-12 (71.3%)
≥ 7.0	103 (8.4%)	2.35e-12 (56.6%)	97 (19.2%)	2.35e-12 (60.4%)	96 (27.7%)	2.34e-12 (65.3%)

Table 3. The success rates for galaxy catalogs generated with different Σ values. The first column gives the Σ values used to generate different galaxy samples, and the following columns give the success rates by number and H α flux. The vertical lines are used to separate the success rates given 3 different H α EW and H α “On” magnitude cuts, where the first group lists rates given no EW nor magnitude cuts, the second group list rates given an EW>7.5 Å, and the third group lists rates given an EW>7.5 Å and magnitudes brighter than 18 mag. We find that our $\Sigma = 2.5$ sample recovers $\sim 24\%$ by number and $\sim 81\%$ by H α flux compared to all galaxies, and that we recover $\sim 68\%$ by number and $\sim 89\%$ by H α flux when comparing to galaxies with an EW and magnitude above our selection limits.

verse. These fainter, new galaxy discoveries suggest that the our effective magnitude limit using single exposure images is marginally deeper than that of the SDSS galaxy survey.

In addition to finding new CLU-H α galaxies fainter than the SDSS magnitude limit we are able to find new galaxies brighter than this limit that were not found by SDSS (see the X’s above the dashed line in Figure 15). The implication of newly discovered bright CLU-H α galaxies suggests that, not only will the CLU-H α survey find fainter galaxies than the SDSS survey, but will also find brighter galaxies missed by the SDSS survey. We expect to find even more new galaxies outside of the SDSS footprint and in an analysis of the deeper, stacked H α images.

To explore the flux limits of this survey, we present the histogram of the spectroscopic H α flux of all known galaxies in Figure 16. In the top panel the unfilled, red-filled, and blue-filled histograms represents all galaxies in the volume, all galaxies in the volume with $\Sigma < 2.5$ (non-candidates), CLU-H α galaxies ($\Sigma \geq 2.5$), and shows that we recover a large fraction of galaxies with higher H α line fluxes. This can be illustrated in the bottom panel of Figure 16 which shows the completeness percentage versus H α line flux (here completeness is defined as the fraction of candidates per all galaxies in each bin of H α line flux). We find that we are 90% and 50% complete at $F_{line} \sim 1 \times 10^{-14}$ and $F_{line} \sim 3 \times 10^{-15}$ (erg/s/cm 2).

4.6 Completeness

In this section we assess the completeness of the CLU-H α galaxy catalog relative to a statistically complete sample of star-forming galaxies, the Local Volume Legacy sample (LVL; Kennicutt et al. 2008; Lee et al. 2009; Dale et al. 2009; Cook et al. 2014a). We quantify our completeness via observable and physical properties, thus providing a robust characterization of galaxies likely found and missed in our survey.

The LVL sample consists of 258 of our nearest galaxy neighbors reflecting a statistically complete, representative sample of the local Universe star-forming galaxies. The fi-

nal LVL sample consists of galaxies that appear outside the Galactic plane ($|b| > 20^\circ$), have a distance less than 11 Mpc ($D \leq 11$ Mpc), span an absolute B -band magnitude of $-9.6 < M_B < -20.7$, and span an RC3 catalog galaxy type range of $-5 < T < 10$. Although the galaxy morphology composition is diverse (i.e., early-type and late-type galaxies), the LVL sample is dominated by dwarf galaxies due to its volume-limited nature. The physical properties of the LVL sample were uniformly measured by Cook et al. (2014b) and are derived from panchromatic (UV-IR) fluxes from GALEX UV, ground-based optical, 2MASS NIR, and Spitzer IR; the physical properties of the CLU-H α galaxies were measured with nearly identical methods (see § 4.3).

We can estimate the completeness of CLU-H α compared to LVL by taking the H α luminosities of LVL, converting them to an H α flux at various distances out to 200 Mpc, and calculate which LVL galaxies are above the CLU-H α flux limit. In this calculation, we use the CLU-H α 90% completeness limit as illustrated in Figure 16, where CLU-H α successfully recovers 90% of all known galaxies in the preliminary fields at $\sim 10^{-14}$ erg/s/cm 2 . At each distance, we measure the fraction of LVL galaxies with an H α flux above the 90% CLU-H α limit, and calculate the following: the number fraction of galaxies, the total H α luminosity, the total B-band luminosity, the total H α SFR, and the total stellar mass. Figure 17 shows the percentage of the LVL galaxies found above the CLU-H α limit versus distance for various properties, where the dotted line, solid blue, blue dashed-dot, red dashed, and blue dashed represent the completeness by number, H α luminosity, B-band luminosity, H α SFR, and stellar mass, respectively.

We find that the completeness by number is nearly 90% at 1 Mpc but drops drastically with distance to 15% at 200 Mpc suggesting that the low-luminosity dwarf galaxies, which dominate this sample, fall below the CLU-H α flux limit. However, the low luminosities of the dwarfs will likely not contribute large fractions of the total luminosities and other physical properties. Figure 17 confirms this conclusion where the limits of CLU-H α continue to recover $>90\%$ in the B-band and H α luminosities as well as the SFR and

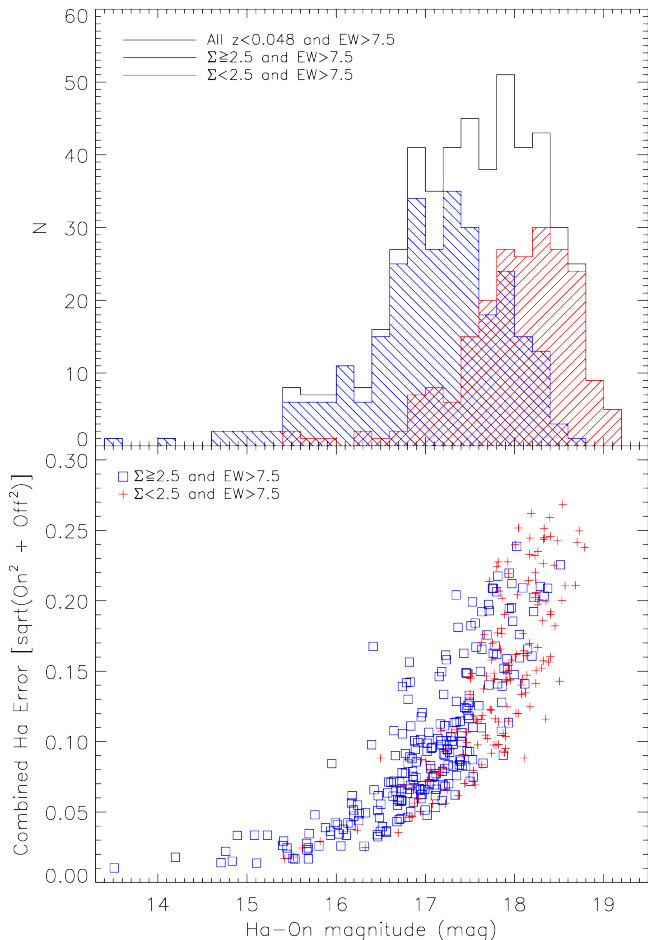


Figure 14. The flux properties all known galaxies in our volume ($z \leq 0.048$) with an $\text{H}\alpha$ $\text{EW} \geq 7.5 \text{ \AA}$, where the blue symbols and histograms represent a subset with $\Sigma \geq 2.5$ (candidates) and the red symbols and histograms represent a subset with $\Sigma < 2.5$ (non-candidates). The top panel shows that the galaxies with a large enough EW to be selected in our survey but not selected as candidates tend to be the fainter objects. The bottom panel shows that these galaxies not selected as candidates also tend to have relatively large combined photometric errors from the “On” and “Off” filters, hence more difficult to be cleanly selected as true emission-line sources.

M_* values out to 100 Mpc. Past 100 Mpc CLU- $\text{H}\alpha$ recovery decreases slowly out to 200 Mpc, but continues to recover $>85\%$ of the total $\text{H}\alpha$ SFR, and $>70\%$ of the total B-band luminosity, $\text{H}\alpha$ luminosity, and stellar mass. We find that the CLU- $\text{H}\alpha$ limits will not recover a large portion of the LVL galaxies out to 200 Mpc due to the many faint dwarfs; however, CLU- $\text{H}\alpha$ will still capture a large fraction of the luminosities and physical properties.

4.7 Comparison to CLU-Compiled Catalog

The CLU- $\text{H}\alpha$ survey was originally designed to contribute to a CLU-compiled catalog to produce one large CLU catalog. Here we examine general properties of the CLU-compiled catalog and explore the contributions of the CLU- $\text{H}\alpha$ galaxies found in our preliminary fields.

The current version of the CLU-compiled catalog contains updates from both NED and SDSS in early 2016. Distances based on Tully-Fischer methods were favored over kinematic (i.e., redshift) distances; however, the majority of the distances are based upon redshift information. In addition to distances, the catalog also contains compiled photometric information. We have cross-matched (within a $4''$ separation) the CLU-compiled catalog with GALEX all sky (Martin et al. 2005), WISE all sky (Wright et al. 2010), and SDSS DR12 (Alam et al. 2015) surveys to obtain fluxes from the ultraviolet (UV) to the infrared (IR), where we found $\sim 154,200$ matches for GALEX FUV, $\sim 216,000$ for WISE 3.4 and $22\mu\text{m}$, and $\sim 100,400$ for SDSS r-band.

We have also derived physical properties for the CLU-compiled galaxies via similar methods as the CLU- $\text{H}\alpha$ survey in §4.3. However, since the final CLU- $\text{H}\alpha$ fluxes have not been generated for the full $\approx 3\pi$ survey, the CLU-compiled catalog does not contain $\text{H}\alpha$ derived SFRs. As a result, we have calculated the recent SFRs (corrected for extinction) of the CLU-compiled galaxies derived from GALEX FUV luminosities via the prescription of Murphy et al. (2011) with the same assumptions as those used to derive the $\text{H}\alpha$ SFRs for the CLU- $\text{H}\alpha$ survey. The FUV luminosities are corrected for extinction using WISE $22\mu\text{m}$ luminosities via the prescription of Hao et al. (2011). Finally, to compare apples-to-apples, we have derived FUV-based SFRs for the CLU- $\text{H}\alpha$ galaxies in the preliminary fields with which we can compare the entire CLU-compiled catalog.

Figure 18 shows the observable and physical property histograms of both the CLU-compiled galaxies (open histogram) and CLU- $\text{H}\alpha$ galaxies in the preliminary fields (blue-filled histogram), where all histograms have been normalized to the peak.

Panel a) shows the SDSS g-r color histograms, where the CLU-compiled sample shows a double peak while the CLU- $\text{H}\alpha$ sample shows a single peak that overlaps with the CLU-compiled blue peak. The double peak is due to the dichotomy between blue star-forming galaxies and red early-type galaxies with little-to-no star formation. The absence of a red peak in the CLU- $\text{H}\alpha$ sample indicates that the CLU- $\text{H}\alpha$ survey is not sensitive to early type galaxies. This is expected since our galaxy selection methods are based on $\text{H}\alpha$ emission which is an indicator of on-going star formation. Thus, the galaxies added by the CLU- $\text{H}\alpha$ survey will be biased towards bluer galaxies with recent star formation.

Panel b) shows the absolute r-band histogram, where both CLU-compiled and CLU- $\text{H}\alpha$ samples show two peaks: one for intrinsically bright galaxies ($r \sim 19$ mag) and one for fainter galaxies ($r \sim 14$ mag). The similar shape in absolute magnitude for both the CLU-compiled and $\text{H}\alpha$ samples suggest that the galaxies added by the CLU- $\text{H}\alpha$ survey will contain both intrinsically bright and faint galaxies.

Panel c) shows the FUV derived SFRs, where both compiled and $\text{H}\alpha$ samples peak near $\text{SFR} \sim 10^{-0.5} \text{ M}_\odot \text{yr}^{-1}$, and both samples show a low-SFR tail out to a $\text{SFR} \sim 10^{-3.5} \text{ M}_\odot \text{yr}^{-1}$. The similar SFR distributions of both the CLU-compiled and $\text{H}\alpha$ samples suggest that the galaxies added by the CLU- $\text{H}\alpha$ survey will sample both high and relatively low-SFRs. We note that the low-SFR tail in the CLU- $\text{H}\alpha$ sample is more sparsely populated compared to the CLU-compiled sample. It is unclear if this is due to a

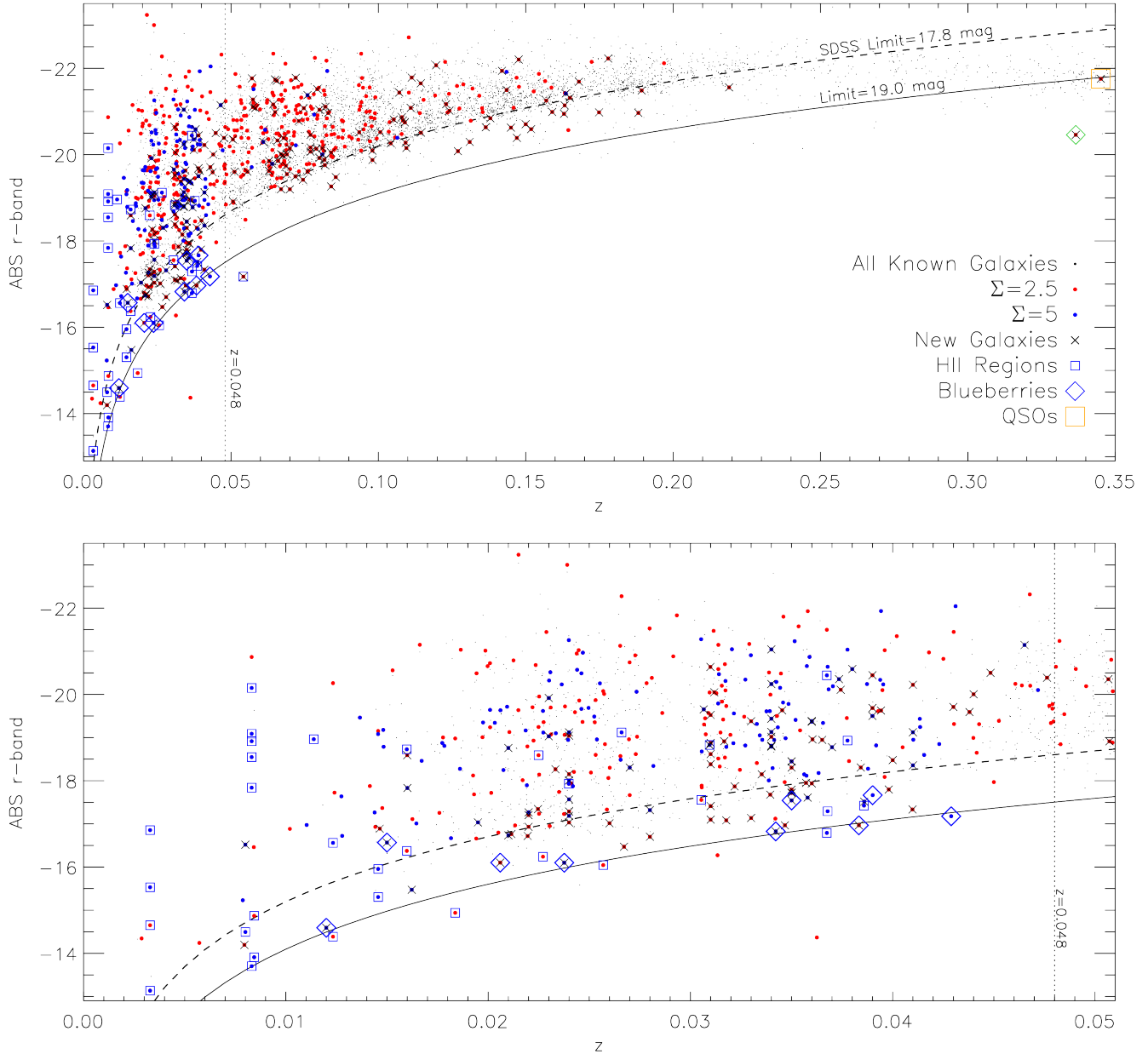


Figure 15. The distribution of absolute r-band magnitude and redshift for all known galaxies and CLU-H α galaxies, where the top panel presents the full redshift range of the CLU-H α candidates while the bottom panel is a zoom-in of the local Universe ($z < 0.05$). The vertical dotted line represents the maximum redshift limit of our survey (i.e., $z = 0.048$), the dashed- and solid-curved lines represent the relationship between an apparent magnitude limit of 17.8 (i.e., the limit of the SDSS spectroscopic galaxy survey) and 19 mag, respectively, with redshift. The small black, larger red, larger blue dots, and X's represent all known galaxies, $\Sigma = 2.5$ CLU-H α galaxies, $\Sigma = 5$ CLU-H α galaxies, and CLU-H α galaxies with no previous distance information (i.e., newly discovered in the local Universe), respectively. We find that the newly discovered CLU-H α galaxies are both fainter and brighter than the SDSS spectroscopic galaxy survey. Thus, we are likely to find many new galaxies even within the SDSS footprint.

selection bias or low number statistics in the preliminary fields.

Panel d) shows the stellar mass histograms, where the CLU-compiled and H α samples span roughly the same mass range and both have a low-mass tail. Thus, the galaxies added by the H α survey will sample similar stellar masses. We note that the low-mass tail of the CLU-compiled sample extends below the tail of the H α sample ($\text{Log}(M_\star) < 7 M_\odot$).

These extremely low-mass galaxies are typically observable only in the Local Group ($D \leq 20$ Mpc) and may not be detected in the H α survey in large numbers past a few 10s of Mpc. Further examination of the stellar mass histograms shows that the CLU-compiled sample peaks at 0.5 dex higher in M_\star than the H α sample indicating an over-abundance of massive elliptical galaxies. The offset in M_\star peak suggests that the new galaxies added by the H α survey

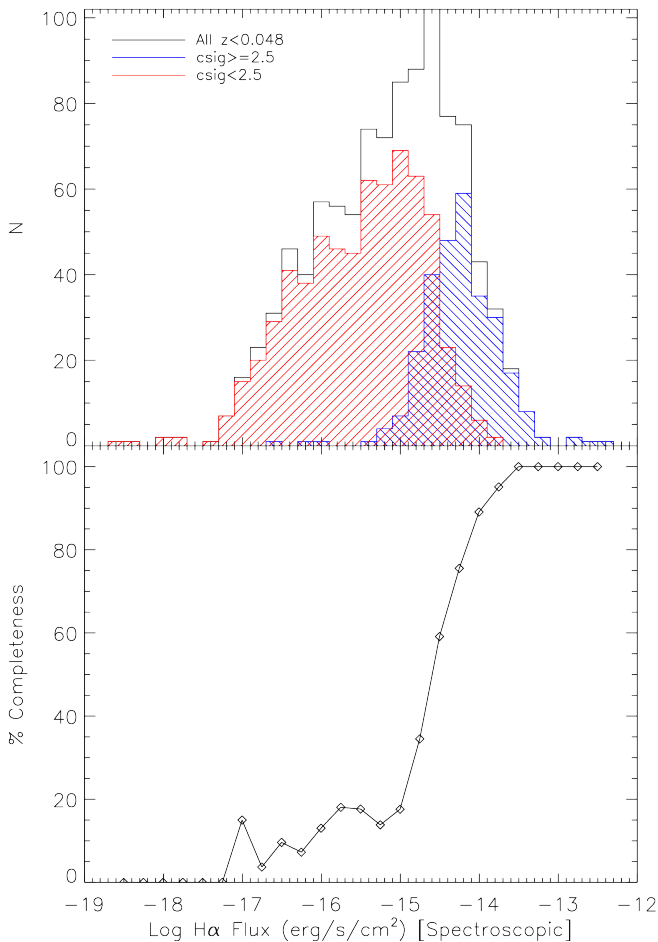


Figure 16. The H α flux histogram and completeness for the CLU-H α galaxies compared to all known galaxies in the same preliminary fields. In the top panel the unfilled, red-filled, and blue-filled histograms represents all galaxies in the volume, all galaxies in the volume with $\Sigma < 2.5$ (non-candidates), CLU-H α galaxies ($\Sigma \geq 2.5$). The bottom panel shows the completeness percentage compared to all known galaxies in each bin of H α flux versus H α flux. The CLU-H α galaxies are 90% complete at $\sim 1 \times 10^{-14}$ erg/s/cm 2 .

will likely not contain massive elliptical galaxies. However, the most massive elliptical galaxies in the local Universe will generally be bright enough to have been previously examined, and it is likely that the distances to these galaxies will also have been measured.

5 DISCUSSION

In this section we examine interesting candidates found in the preliminary fields of the H α survey where we find new blue compact dwarf galaxies (i.e., blueberries), a newly discovered green pea, a new QSO, and a known planetary nebula. We also investigate previously established relationships between different galaxy physical properties (e.g., the star-forming “Main Sequence”) in the CLU-H α galaxy catalog. The majority of the CLU-H α galaxies show physical properties similar to normal star-forming galaxies; however, several

extreme galaxies (i.e., blueberries) show deviations from previously established galaxy trends. The extreme galaxies and interesting candidates found in the preliminary fields show that the CLU-H α survey can have impacts on a wide variety of areas in astrophysical research.

5.1 Interesting Candidates

In this section we provide a detailed examination of some interesting candidates found in the H α preliminary fields. We find that the new blueberry galaxies and new green pea have similar properties with large SFRs and low metallicities. We also find that the new QSO and known planetary nebula have properties similar to other similar objects. However, we note that finding these objects in our candidates list is evidence that the CLU-H α survey can be used to find a variety of extreme objects.

Amongst our emission-line candidates we find interesting candidates that include 9 blue compact dwarfs (i.e., blueberries) 7 of which are new, a new green pea, a new QSO, and a known planetary nebula. Figure 19 presents a mosaic of some of our interesting candidates, where panel a) shows the known planetary nebula, panel b) shows one of the new blueberries, panel c) shows the new green pea, and panel d) shows new QSO. Due to the large “On-Off” magnitudes of the planetary nebula, the central pixels in top panel of Figure 19 in the first H α filter were masked to provide a more consistent background and visual comparison across the four H α images.

We detected the H α emission from a known planetary nebulae. The planetary nebula is PN H 4-1 ($l = 49.3065^\circ$, $b = 88.14757^\circ$. Panel a) of Figure 19 shows the SDSS gri color and our 4 H α filters (in panels from left-to-right, respectively). PN H 4-1 shows large flux excess in H α 1 compared to H α 2 (i.e., “On-Off”) equal to three orders of magnitude ($\Delta\text{mag} = -3.05$). The measured spectroscopic H α line flux and EW are 1.21×10^{-12} erg s $^{-1}$ cm $^{-2}$ and 1200 Å, respectively. The spectra of this PN is shown in top panel of Figure 20, and exhibits emission lines similar to other known planetary nebulae.

The confirmation of this planetary nebula is interesting since our choice of preliminary fields avoided the Galactic plane and PN H 4-1 is located at a Galactic latitude of $\sim 88^\circ$ (i.e., far from the Galactic plane). We anticipate that the CLU-H α survey can be used as a discovery engine for new planetary nebulae inside and outside the Galactic plane. This expectation is based on the Galactic latitude limits ($|b| < 5^\circ$) of the largest H α galactic plane survey to date (IPHAS in the north and VPHAS+ in the south; Drew et al. 2005, 2014). CLU-H α will survey the entire northern Galactic plane.

In the CLU-H α sample, there are 9 (7 newly discovered) blueberry galaxies, or blue compact dwarfs. Panel b) of Figure 19 shows the image cutouts of an example blueberry galaxy that is newly discovered, where the source is brightest in the fourth H α filter. The second panel of Figure 20 shows the spectrum of the blueberry galaxy where the redshifted wavelength of the strong H α line confirms the identification in the fourth filter. The spectra of the example blueberry galaxy is representative of the other blueberry galaxies, where both the [OIII] $\lambda 4959, \lambda 5007$ and H α lines exhibit strong emission lines: 418 Å and 446 Å for

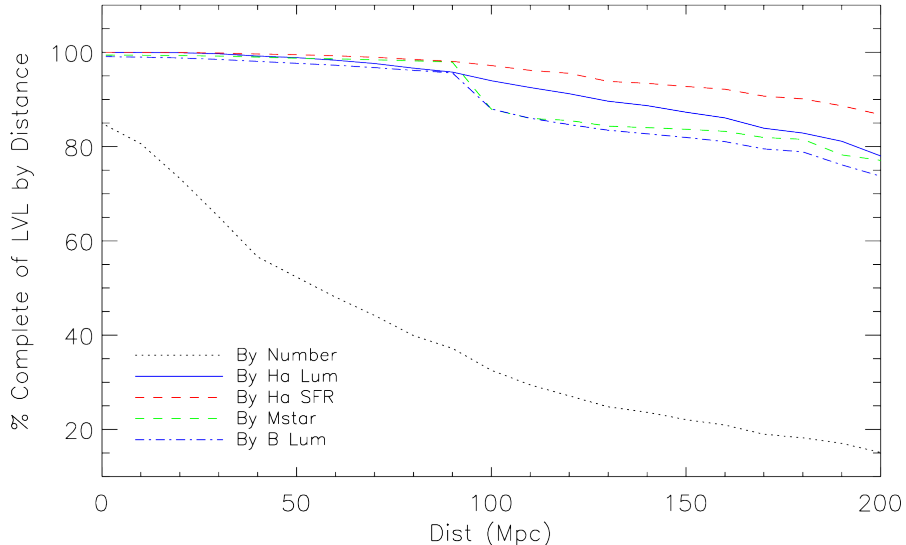


Figure 17. The completeness of the CLU-H α galaxies versus distance as compared to a statistically complete sample of nearby ($D \leq 11$ Mpc) star-forming galaxies (LVL). Completeness is defined by the fraction of LVL galaxies that can be detected in the CLU-H α survey at different distances given the CLU-H α 90% H α flux completeness of $\sim 10^{-14}$ erg/s/cm 2 . We find that CLU-H α will recover the following LVL properties: 85% by H α SFR, 75% by stellar mass, and 15% by number at 200 Mpc.

[OIII] $\lambda 4959, \lambda 5007$ and H α , respectively. We measure the 12+Log(O/H) metallicity of 8.02 from O3N2 methods (Pettini & Pagel 2004) and a dust corrected SFR of $0.41 M_{\odot} \text{ yr}^{-1}$.

The SDSS and CLU-H α images of the newly discovered green pea are shown in panel c) of Figure 19. The spectra of this object is shown in third panel of Figure 20 where the [OIII] $\lambda 4959, \lambda 5007$ lines confirm the correct identification in the H $\alpha 3$ filter. Both the [OIII] $\lambda 4959, \lambda 5007$ and H α lines exhibit strong emission lines: 510 Å and 560 Å for [OIII] $\lambda 4959, \lambda 5007$ and H α , respectively. We have measured metallicity of 12+log(O/H) = 8.09 via the O3N2 method. The H α flux of $9. \times 10^{-15}$ erg/s/cm 2 indicates a dust corrected SFR of $24 M_{\odot} \text{ yr}^{-1}$ given the measured redshift of 0.337 and H $_0$ of 72 km/s/Mpc. The green pea emission lines are similar in strength to that of the blueberries. In addition, both the green pea and example blueberry exhibit similar low metallicities. Thus, it is likely that these two types of galaxies are related.

The image cutouts of the new QSO found in our survey of preliminary fields is shown in panel d) of Figure 19 where the QSO is brightest in the third H α filter. In addition, the spectrum of this object is shown in the bottom panel of Figure 20 which shows strong [OIII] $\lambda 4959, \lambda 5007$ lines confirming the correct identification in our third filter. Furthermore, the broadened H α and H β emission lines clearly indicate the presence of a strong AGN at the center of this galaxy. The spectrum of this QSO is similar to other QSO spectra.

5.2 Galaxy Trends

In this section we investigate established trends of star-forming galaxies. Previous studies of star-forming galaxies have found a relatively tight correlation between the current SFR and the total stellar mass for both local Universe and

higher redshift galaxy samples: the galaxy “Main Sequence”. The galaxy “Main Sequence” can provide insights into how galaxies evolve over time since the “Main Sequence” normalization increases with redshift (e.g., Heinis et al. 2014).

Figure 21 shows the H α -derived SFR versus stellar mass (M_{\star}) for the CLU-H α galaxies, where the symbols are the same as those in Figure 15. The blue and green lines represents the relationships found in the LVL sample ($D < 11$ Mpc; Cook et al. 2014b) and SDSS sample ($z \sim 0.1$; Peng et al. 2010). The majority of the CLU-H α galaxies follow the previous “Main Sequence” relationship and span a wide range in both SFR and stellar mass from low-mass, low-SFR dwarfs to high-mass, high-SFR spirals.

The blueberry galaxies found in the CLU-H α sample show high SFRs given their stellar masses suggesting that these galaxies are undergoing an episode of enhanced star formation. The new green pea, on the other hand, shows good agreement with the SDSS “Main Sequence” relationship suggesting that this galaxy is not undergoing an enhanced period of star formation; this is contradictory to previous studies which find that green peas show signs of significant star formation activity (Cardamone et al. 2009; Izotov, Guseva & Thuan 2011). However, we note that the image cutouts of the green pea in Figure 19 shows nearby sources which could be contaminating the WISE1 flux due to the relatively large PSF of the WISE instrument (6" at $3.4\mu\text{m}$). Thus, it is possible that our stellar mass may be an overestimate, which, if true, would move the green position to the left on the “Main Sequence” plot resulting a high SFR for its stellar mass.

We also explore a relationship between physical and observed properties of galaxies, where local Universe studies have found that the specific SFR ($s\text{SFR} \equiv \text{SFR}/M_{\star}$) forms a relatively tight trend with optical colors (e.g., Cook et al. 2014b; Schawinski et al. 2014). In the LVL sample of 258

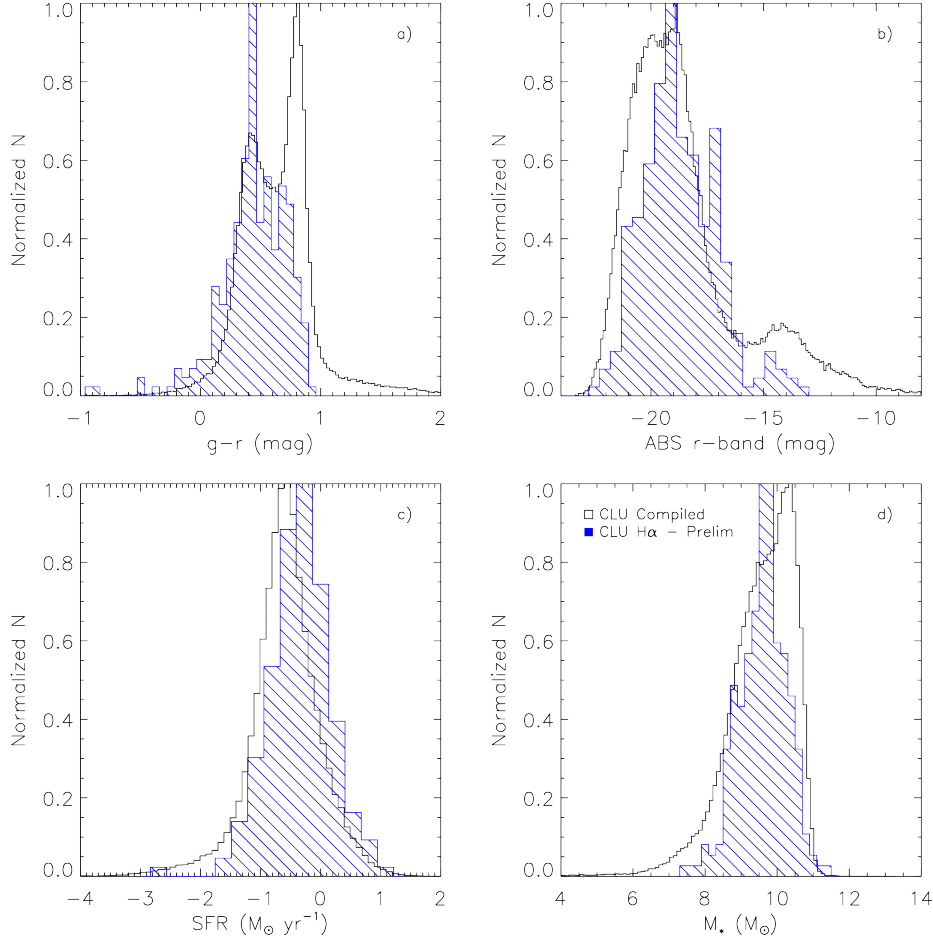


Figure 18. A Comparison observable and physical properties between the CLU-compiled (all known galaxies with $z < 0.048$) and CLU-H α galaxy samples, where panels a, b, c, and d show the histograms of g-r color, absolute r-band magnitude, FUV-derived SFR, and stellar mass, respectively. We find that both the compiled and H α samples show similar distributions except for g-r color and stellar mass, where the CLU-H α sample shows reduced numbers of optically red and massive galaxies. Since the H α survey is based on an H α emission line that indicates recent star formation, it is likely that red massive galaxies with little-to-no on-going star formation will be missed. However, these bright galaxies will likely have been characterized in previous galaxy survey.

nearby galaxies, Cook et al. (2014b) found that dwarfs and irregular galaxies tended to have higher sSFR and bluer colors while later-type and elliptical galaxies tended to have lower sSFRs and redder colors. The sSFR of a galaxy is an indicator of the intensity of star formation; thus, can provide insights into the population of the CLU-H α galaxies.

Figure 22 shows the sSFR versus the SDSS g-r color of the CLU-H α galaxies, where the symbols are the same as that in Figure 21. We find that the CLU-H α galaxies follow a similar trend to the LVL galaxies. However, the CLU-H α blueberry galaxies tend to have some of the highest sSFRs and bluest optical colors with sSFRs as high as -8.7 in Log(sSFR), whereas the highest sSFR of the LVL galaxies is -9.5 in Log(sSFR). In addition, the partial separation of the blueberry galaxies and the rest of the CLU-H α galaxies suggests that these galaxies are forming stars with high intensities compared to normal star-forming galaxies.

The new green pea galaxy shows a sSFR and color similar to that of the CLU-H α galaxies indicating that this green pea is forming stars with a similar intensity to normal

star-forming galaxies. However, as mentioned previously, the green pea M_* may be overestimated; thus, it is possible that the sSFR may be underestimated. Future studies of CLU-H α galaxies will include larger numbers of green pea galaxies.

5.3 Future Improvements

Future improvements to maximize the completeness and minimize the contamination of the CLU-H α catalog include: (i) Stacking all H α images to produce a deeper H α source catalog and a resulting deeper galaxy catalog. These data will, not only, provide deeper images from which to find more galaxies, but will also facilitate removal of cosmic rays and chip defects. (ii) Extended source photometry; (iii) Machine learning for star-galaxy separation; (iv) Image subtraction of “On” and “Off” filters.

In addition, efforts to use machine learning for candidate selection are currently underway. The preliminary CLU-H α survey fields are critical to our machine learning

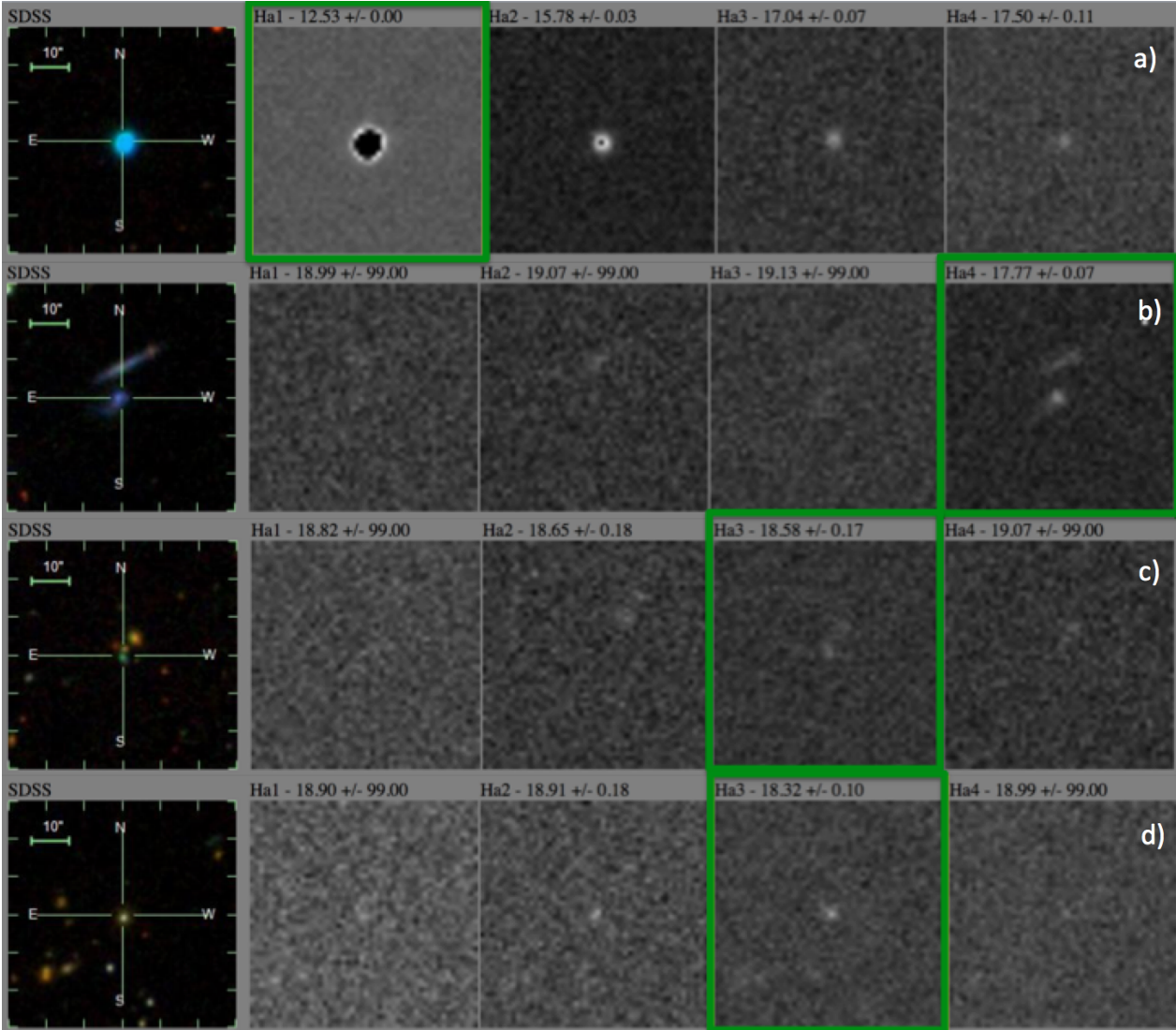


Figure 19. A mosaic of some interesting candidates found in our preliminary fields similar to Figure 11. Panels a-d shows the known planetary nebula, an example of a new blueberry, the new green pea, and the new QSO, respectively. In addition, the thin galaxy just above center in panel b) is also newly discovered CLU-H α galaxy with an H α EW=80 Å.

efforts as they establish a training set of objects with known redshifts. We have run preliminary tests on how well our machine learning algorithms perform the tasks of classifying objects as simply within 200 Mpc and classifying objects as within one of our narrowband filters. Preliminary results are promising, showing that we can increase our completeness by using our current metrics along with additional information (e.g., Pan-STARRS, WISE, GALEX magnitudes) as features in our machine learning algorithms (Zhang et al. 2018; in prep).

6 SUMMARY

In this paper we have presented the Census of the Local Universe (CLU) project which endeavors to build the most complete list of galaxies with measured distances less than 200 Mpc. The full CLU galaxy catalog is a combi-

nation of all known galaxies compiled from many existing catalogs (CLU-compiled; 234,500 galaxies) and the largest area ($\approx 3\pi$) narrowband imaging survey that deploys 4 filters to search for galaxies with H α emission out to 200 Mpc (CLU-H α). The motivation for the CLU project is to build a galaxy catalog that can focus the observational follow-up efforts that search for electromagnetic counterparts to gravitational wave events detected by LIGO-Virgo. However, CLU-H α can also be used for star formation and galaxy evolution studies since our narrowband imaging provides nearly uniform H α fluxes (and subsequently star formation rates) across $\approx 3\pi$ of the sky.

The CLU-H α survey has imaged 26,470 square degrees of the northern sky above -20° declination using four narrowband filters with a FWHM of 75–90 Å and a wavelength range of 6525–6878 Å (out to $z=0.048$). The observations utilize 3 spatially staggered grids where each grid has 3626 fields. The first two filters cover the galactic plane and the

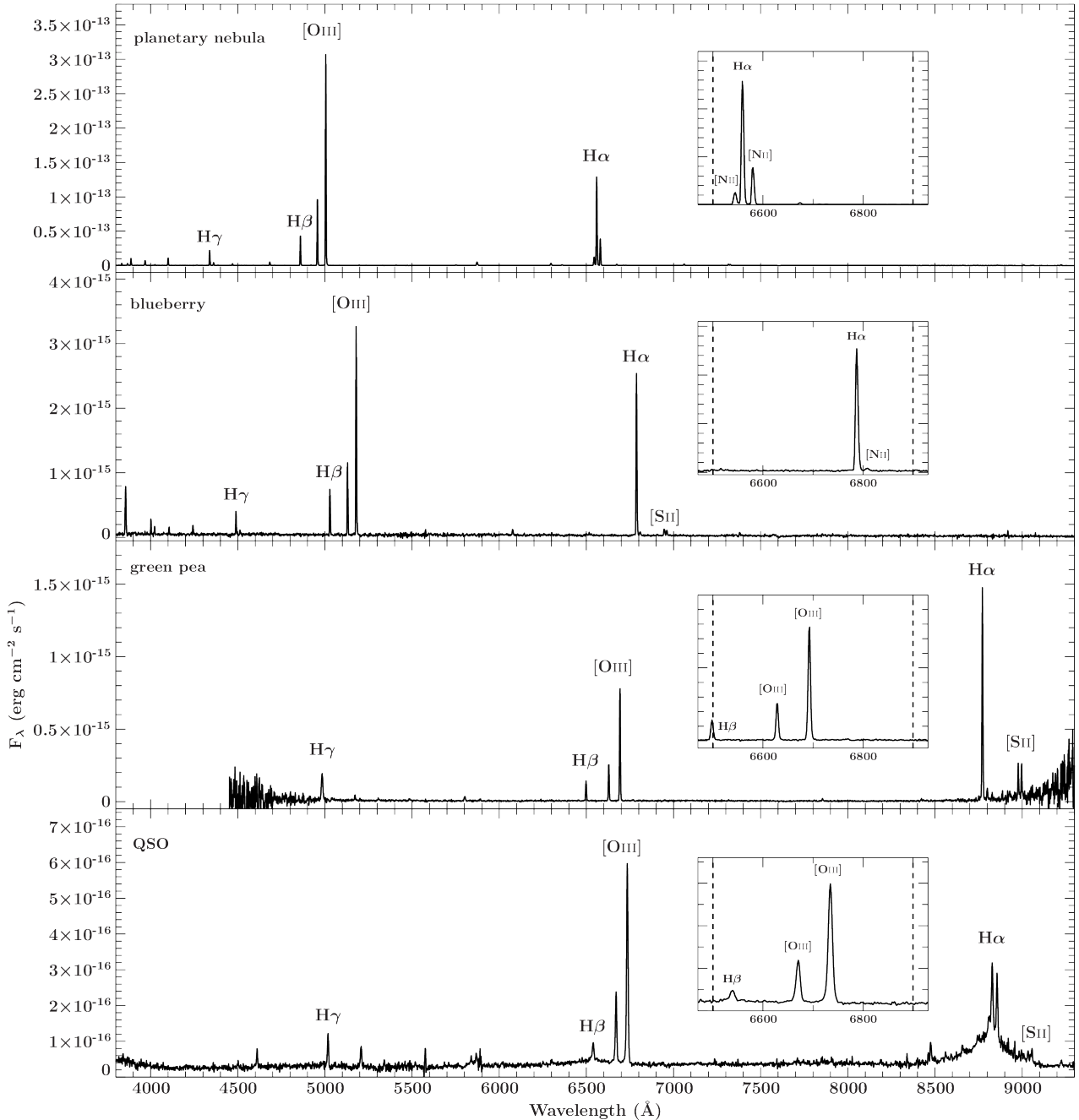


Figure 20. The Palomar DBSP spectra for the interesting candidates found in our preliminary fields where (from top-to-bottom) the panels display the known planetary nebula, an example of one newly discovered blueberry, the new green pea, and the new QSO. Strong nebular lines are labeled in each panel. The inserts in each panel show a zoomed-in window where the vertical dashed lines represent the wavelength range covered by our narrowband filter (6500–6900 Å).

last two filters avoid the galactic plane ($|b| \gtrsim 3^\circ$). The analysis of CLU-H α fields in this study utilize only 14 preliminary fields ($\approx 100 \text{ deg}^2$) in one of spatially staggered grids, but future studies will examine larger sky coverages and finally the full $\approx 3\pi$ area with 3 stacked images on every point in the CLU-H α survey area.

In the 14 preliminary fields we use standard signal-to-noise selection methods to quantify the presence of an emission-line via narrowband color excess significance (Σ). In addition, we undertook a spectroscopic follow-up cam-

paign at Palomar Observatory and WIRO to obtain redshifts of all galaxy candidates with $\Sigma \geq 2.5$ and no previous redshift information ($N=334$). These redshifts allow us to explore the composition of our galaxy candidates at different Σ cuts. There are 290 galaxies found in the correct filter with 40% contamination for $\Sigma \geq 2.5$, and 151 confirmed galaxies and 7.1% contamination for $\Sigma \geq 5$. We conclude that $\Sigma = 2.5$ cut produces a more complete catalog of galaxies in our local volume but higher contamination while $\Sigma = 5$ cut produces a high fidelity galaxy catalog where the ma-

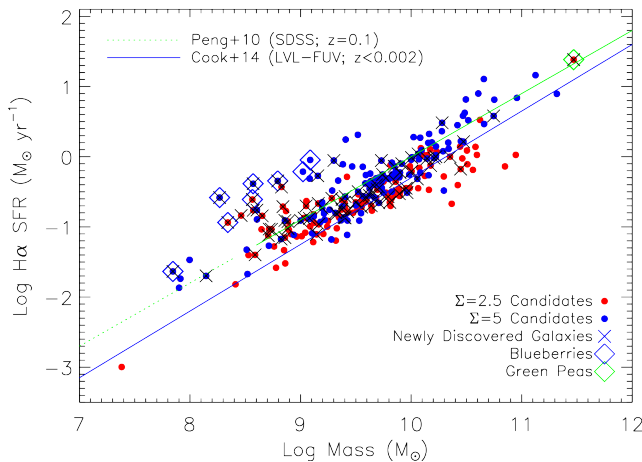


Figure 21. The “Main Sequence” of star-forming galaxies where there exists a relationship between current $\text{H}\alpha$ derived SFR and total stellar mass (M_\star). The red dots, blue dots, large X’s represent $\Sigma = 2.5$ CLU- $\text{H}\alpha$ galaxies, $\Sigma = 5$ CLU- $\text{H}\alpha$ galaxies, and newly discovered CLU- $\text{H}\alpha$ galaxies in the local Universe. The blue and green lines represents the relationships found in the LVL sample ($D < 11$ Mpc; Cook et al. 2014b) and SDSS sample ($z \sim 0.1$; Peng et al. 2010). The green soliddotted line transition represents the lower end of the stellar mass range probed by the SDSS survey. We find that the majority of the CLU- $\text{H}\alpha$ galaxies show agreement with the local Universe “Main Sequence”. In addition, the blue and green diamonds represent the blueberry and green pea galaxies found in our preliminary fields. These extreme galaxies show higher SFRs for their given stellar mass.

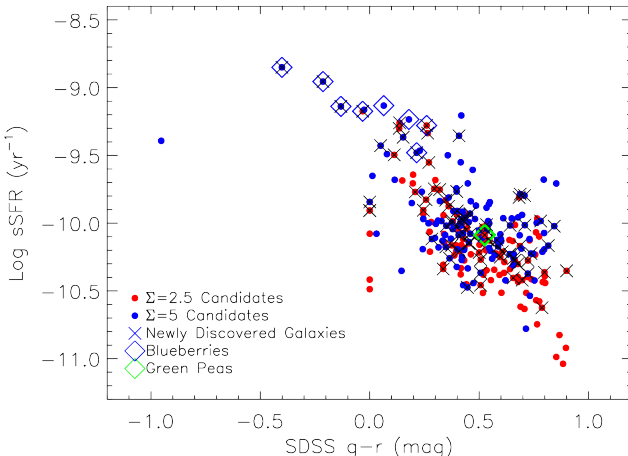


Figure 22. The specific star formation rate ($\text{sSFR} \equiv \text{SFR}/M_\star$) versus $\text{g}-\text{r}$ optical color, where sSFR is an indicator for the intensity of star formation. We find that the blueberry galaxies show the highest star formation rate intensities (sSFR) and tend to have the bluest colors. The new green pea galaxy shows a sSFR similar to other normal star-forming galaxies. However, the low sSFR could be attributed to an overestimate of the stellar mass due to contaminating light in the WISE1 aperture.

jority of candidates are galaxies found in the correct filter with little contamination. We will release a table of all candidates above a $\Sigma = 2.5$ cut in the electronic version of this publication.

In addition, we use the 14 preliminary fields to examine the limits and completeness of CLU- $\text{H}\alpha$ survey. The median 5σ detection limit for a points source in the narrowband imaging is 18.5 mag. A comparison of $\text{H}\alpha$ fluxes derived from narrowband imaging and spectroscopy show good agreement for the majority of galaxies, but reveal different flux limits for different Σ cut values: 2 and 4×10^{-15} erg/s/cm 2 for $\Sigma = 2.5$ and $\Sigma = 5$, respectively. The different flux limits are the result of our selection methods and translate into an apparent $\text{H}\alpha$ magnitudes of 18.3 and 18.0 for the $\Sigma = 2.5$ and $\Sigma = 5$, respectively.

The limits presented in the previous paragraph represent the limit of our selection methods to detect an $\text{H}\alpha$ emission line. However, a comparison to the known galaxies in our preliminary fields shows that we recover 90% of the $\text{H}\alpha$ flux located in the known galaxies at 1×10^{-14} erg/s/cm 2 . Given this limit, we assess our completeness via a comparison to a statistically complete sample of star-forming galaxies (The LVL sample) and find that CLU- $\text{H}\alpha$ will be 85% and 70% complete by $\text{H}\alpha$ -derived SFR and stellar mass at 200 Mpc.

We have cross-matched the resulting CLU- $\text{H}\alpha$ galaxies to GALEX and WISE to derive the physical properties (extinction corrected SFR and stellar mass). We find that the CLU- $\text{H}\alpha$ galaxies span a range in both SFR and stellar mass including dwarf galaxies (i.e., $M_\star \sim 10^8 M_\odot$ and $\text{SFR} \sim 10^{-2} M_\odot \text{ yr}^{-1}$) as well as larger spirals (i.e., $M_\star \sim 10^{11} M_\odot$ and $\text{SFR} \sim 10^1 M_\odot \text{ yr}^{-1}$). We also examine previously established galaxy trends, where we find that the majority of the CLU- $\text{H}\alpha$ galaxies show agreement with galaxy “Main Sequence” trends found in the local Universe. However, we do find some extreme galaxies that lie above the “Main Sequence” trend and some of the highest sSFRs in the CLU- $\text{H}\alpha$ sample.

Within the 14 preliminary fields, we find several interesting objects: 7 newly discovered blue compact dwarfs (aka, blueberries), 1 new green pea, 1 new QSO, and a known planetary nebula. The extreme galaxies (green pea and blueberries) have high star formation rates, low stellar masses, and low metallicities and could be local analogs to higher redshift primordial galaxies. The existence of these objects in our preliminary $\text{H}\alpha$ sample exemplifies that the full CLU- $\text{H}\alpha$ survey would serve as a discovery machine for a wide variety of objects in our own Galaxy and for extreme galaxies out to intermediate redshifts.

REFERENCES

- Aasi J. et al., 2015, Classical and Quantum Gravity, 32, 074001
- Abazajian K. N. et al., 2009, ApJS, 182, 543
- Abbott B. P. et al., 2016, Physical Review Letters, 116, 061102
- Alam S. et al., 2015, ApJS, 219, 12
- Amorín R. O., Pérez-Montero E., Vilchez J. M., 2010, ApJ, 715, L128

- Barnes K. L., van Zee L., Dale D. A., Staudaher S., Bullock J. S., Calzetti D., Chandar R., Dalcanton J. J., 2014, *ApJ*, 789, 126
- Bellm E. C., Sesar B., 2016, pyraf-dbsp: Reduction pipeline for the Palomar Double Beam Spectrograph. Astrophysics Source Code Library
- Bertin E., 2006, in Astronomical Society of the Pacific Conference Series, Vol. 351, Astronomical Data Analysis Software and Systems XV, Gabriel C., Arviset C., Ponz D., Enrique S., eds., p. 112
- Bertin E., Arnouts S., 1996, *A&AS*, 117, 393
- Bianchi L., Conti A., Shiao B., 2014, VizieR Online Data Catalog, 2335
- Brinchmann J., Charlot S., White S. D. M., Tremonti C., Kauffmann G., Heckman T., Brinkmann J., 2004, *MNRAS*, 351, 1151
- Bunker A. J., Warren S. J., Hewett P. C., Clements D. L., 1995, *MNRAS*, 273, 513
- Calzetti D. et al., 2010, *ApJ*, 714, 1256
- Cardamone C. et al., 2009, *MNRAS*, 399, 1191
- Chambers K. C. et al., 2016, ArXiv e-prints
- Cook D. O. et al., 2014a, *MNRAS*, 445, 881
- Cook D. O. et al., 2014b, *MNRAS*, 445, 899
- Daddi E. et al., 2007, *ApJ*, 670, 156
- Dale D. A. et al., 2009, *ApJ*, 703, 517
- Dale D. A., Giovanelli R., Haynes M. P., Campusano L. E., Hardy E., 1999, *AJ*, 118, 1489
- Drew J. E. et al., 2014, *MNRAS*, 440, 2036
- Drew J. E. et al., 2005, *MNRAS*, 362, 753
- Elbaz D. et al., 2007, *A&A*, 468, 33
- Eskew M., Zaritsky D., Meidt S., 2012, *AJ*, 143, 139
- Finkelstein S. L. et al., 2012, *ApJ*, 758, 93
- Fujita S. S. et al., 2003, *The Astrophysical Journal Letters*, 586, L115
- Fukugita M. et al., 2007, *AJ*, 134, 579
- Hao C.-N., Kennicutt R. C., Johnson B. D., Calzetti D., Dale D. A., Moustakas J., 2011, *ApJ*, 741, 124
- Haynes M. P. et al., 2011, *AJ*, 142, 170
- Heinis S. et al., 2014, *MNRAS*, 437, 1268
- Izotov Y. I., Guseva N. G., Thuan T. X., 2011, *ApJ*, 728, 161
- Jarrett T. H. et al., 2013, *AJ*, 145, 6
- Jones D. H. et al., 2009, *MNRAS*, 399, 683
- Kasliwal M. M. et al., 2016, ArXiv e-prints
- Kennicutt R. C., Evans N. J., 2012, *ARA&A*, 50, 531
- Kennicutt, Jr. R. C., 1998, *ARA&A*, 36, 189
- Kennicutt, Jr. R. C., Lee J. C., Funes, José G. S. J., Sakai S., Akiyama S., 2008, *ApJS*, 178, 247
- Kopparapu R. K., Hanna C., Kalogera V., O’Shaughnessy R., González G., Brady P. R., Fairhurst S., 2008, *ApJ*, 675, 1459
- Kroupa P., 2001, *MNRAS*, 322, 231
- Laher R. R. et al., 2014, *PASP*, 126, 674
- Law N. M. et al., 2009, *Publications of the Astronomical Society of the Pacific*, 121, 1395
- Lee J. C. et al., 2011, *ApJS*, 192, 6
- Lee J. C. et al., 2009, *ApJ*, 706, 599
- Lee J. C. et al., 2012, *PASP*, 124, 782
- Lintott C. J. et al., 2008, *MNRAS*, 389, 1179
- Ly C., Lee J. C., Dale D. A., Momcheva I., Salim S., Staudaher S., Moore C. A., Finn R., 2010, *The Astrophysical Journal*, 726, 109
- Makarov D., Prugniel P., Terekhova N., Courtois H., Vauglin I., 2014, *A&A*, 570, A13
- Martin D. C. et al., 2005, *ApJ*, 619, L1
- McGaugh S. S., Schombert J. M., 2014, *AJ*, 148, 77
- McGaugh S. S., Schombert J. M., 2015, *ApJ*, 802, 18
- Meidt S. E. et al., 2014, *ApJ*, 788, 144
- Monet D. G. et al., 2003, *AJ*, 125, 984
- Murphy E. J. et al., 2011, *ApJ*, 737, 67
- Noeske K. G. et al., 2007, *ApJ*, 660, L43
- Norris M. A., Meidt S., Van de Ven G., Schinnerer E., Groves B., Querejeta M., 2014, *ApJ*, 797, 55
- Ofek E. O. et al., 2012, *Publications of the Astronomical Society of the Pacific*, 124, 854
- Oh S.-H., de Blok W. J. G., Walter F., Brinks E., Kennicutt, Jr. R. C., 2008, *AJ*, 136, 2761
- Oke J. B., Gunn J. E., 1982, *PASP*, 94, 586
- Pascual S., Gallego J., Arag n Salamanca A., Zamorano J., 2001, *Astronomy and Astrophysics*, 379, 798
- Peng Y.-j. et al., 2010, *ApJ*, 721, 193
- Pettini M., Pagel B. E. J., 2004, *MNRAS*, 348, L59
- Querejeta M. et al., 2015, *ApJS*, 219, 5
- Rau A. et al., 2009, *PASP*, 121, 1334
- Salim S. et al., 2007, *ApJS*, 173, 267
- Schawinski K. et al., 2014, *MNRAS*
- Schlafly E. F., Finkbeiner D. P., 2011, *ApJ*, 737, 103
- Sobral D. et al., 2009, *Monthly Notices of the Royal Astronomical Society*, 398, 75
- Stroe A., Sobral D., 2015, *MNRAS*, 453, 242
- Tully R. B., Rizzi L., Shaya E. J., Courtois H. M., Makarov D. I., Jacobs B. A., 2009, *AJ*, 138, 323
- White M. et al., 2011, *ApJ*, 728, 126
- Wright E. L. et al., 2010, *AJ*, 140, 1868
- York D. G. et al., 2000, *AJ*, 120, 1579
- Zacharias N. et al., 2010, *AJ*, 139, 2184

ACKNOWLEDGEMENTS

This work was supported by the GROWTH (Global Relay of Observatories Watching Transients Happen) project funded by the National Science Foundation under PIRE Grant No 1545949.

This research has made use of the NASA/IPAC Extragalactic Database (NED) which is operated by the Jet Propulsion Laboratory, California Institute of Technology, under contract with the National Aeronautics and Space Administration. This publication makes use of data products from the Wide-field Infrared Survey Explorer, which is a joint project of the University of California, Los Angeles, and the Jet Propulsion Laboratory/California Institute of Technology, funded by the National Aeronautics and Space Administration.

The Pan-STARRS1 Surveys (PS1) and the PS1 public science archive have been made possible through contributions by the Institute for Astronomy, the University of Hawaii, the Pan-STARRS Project Office, the Max-Planck Society and its participating institutes, the Max Planck Institute for Astronomy, Heidelberg and the Max Planck Institute for Extraterrestrial Physics, Garching, The Johns Hopkins University, Durham University, the University of Edinburgh, the Queen’s University Belfast, the Harvard-Smithsonian Center for Astrophysics, the Las Cumbres Ob-

servatory Global Telescope Network Incorporated, the National Central University of Taiwan, the Space Telescope Science Institute, the National Aeronautics and Space Administration under Grant No. NNX08AR22G issued through the Planetary Science Division of the NASA Science Mission Directorate, the National Science Foundation Grant No. AST-1238877, the University of Maryland, Eotvos Lorand University (ELTE), the Los Alamos National Laboratory, and the Gordon and Betty Moore Foundation.

Funding for SDSS-III has been provided by the Alfred P. Sloan Foundation, the Participating Institutions, the National Science Foundation, and the U.S. Department of Energy Office of Science. The SDSS-III web site is <http://www.sdss3.org/>.

SDSS-III is managed by the Astrophysical Research Consortium for the Participating Institutions of the SDSS-III Collaboration including the University of Arizona, the Brazilian Participation Group, Brookhaven National Laboratory, Carnegie Mellon University, University of Florida, the French Participation Group, the German Participation Group, Harvard University, the Instituto de Astrofisica de Canarias, the Michigan State/Notre Dame/JINA Participation Group, Johns Hopkins University, Lawrence Berkeley National Laboratory, Max Planck Institute for Astrophysics, Max Planck Institute for Extraterrestrial Physics, New Mexico State University, New York University, Ohio State University, Pennsylvania State University, University of Portsmouth, Princeton University, the Spanish Participation Group, University of Tokyo, University of Utah, Vanderbilt University, University of Virginia, University of Washington, and Yale University.

Preliminary Fields Properties

Field (name)	RA center (J2000)	DEC center (J2000)	Filter (name)	Obs-Date	5σ Detection Limit (AB mag)	EW Limit $\Sigma=2.5$ (Å)	EW Limit $\Sigma=5$ (Å)
p3967	13:01:56.1	28:07:30.0	H α 1	2012-05-09	18.59 \pm 0.12	7.74	16.27
			H α 2	2012-05-09	18.73 \pm 0.12	7.97	16.76
			H α 3	2015-06-02	18.63 \pm 0.17	9.41	19.78
			H α 4	2015-06-02	18.54 \pm 0.14	9.44	19.85
p4063	14:06:35.6	30:22:30.0	H α 1	2014-02-15	18.61 \pm 0.18	7.06	14.77
			H α 2	2014-02-15	18.61 \pm 0.18	7.27	15.22
			H α 3	2015-02-04	18.87 \pm 0.19	9.27	19.47
			H α 4	2015-02-04	18.92 \pm 0.19	9.30	19.54
p4064	14:22:25.1	30:22:30.0	H α 1	2014-02-15	18.43 \pm 0.18	8.09	17.03
			H α 2	2014-02-15	18.61 \pm 0.17	8.33	17.54
			H α 3	2015-02-04	18.88 \pm 0.18	7.87	16.42
			H α 4	2015-02-04	18.96 \pm 0.20	7.90	16.47
p4070	15:57:21.8	30:22:30.0	H α 1	2013-03-26	18.65 \pm 0.19	6.17	12.85
			H α 2	2013-03-26	18.97 \pm 0.19	6.36	13.24
			H α 3	2015-07-01	18.65 \pm 0.13	6.75	13.99
			H α 4	2015-07-01	18.62 \pm 0.14	6.77	14.03
p4071	16:13:11.2	30:22:30.0	H α 1	2013-03-26	18.95 \pm 0.20	6.05	12.59
			H α 2	2013-03-26	19.07 \pm 0.20	6.24	12.97
			H α 3	2015-07-01	18.45 \pm 0.13	8.27	17.29
			H α 4	2015-07-01	18.56 \pm 0.14	8.30	17.34
p4072	16:29: 0.7	30:22:30.0	H α 1	2013-03-26	19.00 \pm 0.20	5.91	12.27
			H α 2	2013-03-26	19.07 \pm 0.20	6.08	12.64
			H α 3	2015-09-28	19.28 \pm 0.28	9.51	20.00
			H α 4	2015-09-28	19.06 \pm 0.27	9.54	20.07
p4073	16:44:50.1	30:22:30.0	H α 1	2013-03-26	19.01 \pm 0.21	5.79	12.02
			H α 2	2013-03-26	18.91 \pm 0.19	5.97	12.38
			H α 3	2015-09-27	18.86 \pm 0.13	7.80	16.27
			H α 4	2015-09-27	18.84 \pm 0.15	7.83	16.32
p4074	17:00:39.6	30:22:30.0	H α 1	2013-04-29	18.88 \pm 0.19	6.65	13.87
			H α 2	2013-04-29	18.96 \pm 0.18	6.85	14.29
			H α 3	2015-08-01	19.01 \pm 0.16	8.05	16.82
			H α 4	2015-08-01	19.12 \pm 0.16	8.08	16.87
p4075	17:16:29.0	30:22:30.0	H α 1	2013-04-29	18.75 \pm 0.20	7.27	15.23
			H α 2	2013-04-29	18.88 \pm 0.17	7.49	15.69
			H α 3	2015-08-01	19.01 \pm 0.14	10.39	21.95
			H α 4	2015-08-01	18.89 \pm 0.24	10.42	22.02
p4095	22:32:58.0	30:22:30.0	H α 1	2013-05-24	18.33 \pm 0.17	6.58	13.72
			H α 2	2013-05-24	18.47 \pm 0.18	6.77	14.13
			H α 3	2015-09-29	18.77 \pm 0.15	7.98	16.64
			H α 4	2015-09-29	18.78 \pm 0.17	8.00	16.70
p4096	22:48:47.5	30:22:30.0	H α 1	2013-06-21	19.00 \pm 0.31	6.74	14.07
			H α 2	2013-06-21	19.14 \pm 0.29	6.94	14.49
			H α 3	2015-10-26	18.61 \pm 0.15	6.82	14.15
			H α 4	2015-10-26	18.57 \pm 0.16	6.84	14.20
p4098	23:20:26.4	30:22:30.0	H α 1	2013-06-21	19.05 \pm 0.29	6.52	13.61

Table Continued

			H α 2	2013-06-21	19.03 ± 0.30	6.72	14.02
			H α 3	2015-10-29	18.67 ± 0.13	8.15	17.01
			H α 4	2015-10-29	18.70 ± 0.14	8.17	17.07
p4192	00:41:22.8	34:52:30.0	H α 1	2014-02-14	18.41 ± 0.19	6.92	14.47
			H α 2	2014-02-14	18.58 ± 0.17	7.13	14.91
			H α 3	2015-09-26	18.84 ± 0.19	7.41	15.43
			H α 4	2015-09-26	18.85 ± 0.20	7.44	15.48
p4193	00:57:55.9	34:52:30.0	H α 1	2014-02-14	18.50 ± 0.16	6.68	13.94
			H α 2	2014-02-14	18.59 ± 0.17	6.88	14.36
			H α 3	2015-02-03	18.33 ± 0.13	7.22	15.02
			H α 4	2015-02-03	18.65 ± 0.16	7.25	15.07

Table 4: The basic properties of the 14 preliminary fields analyzed here. The first three columns list the name and central coordinates of the 14 preliminary fields followed by the basic information of the four H α filters in each pointing. The information listed for the four H α filters are from left-to-right: the filter name, the observation date, the median and standard deviation 5σ detection limits for the 11 chips in the pointing, the EW limit for the $\Sigma = 2.5$ and $\Sigma = 5$ limits set by the scatter in bright continuum sources as seen in the color-magnitude diagrams of Figures 5-8.